

E9744  
12-7-95

NASA Contractor Report 195456

# PARC3D Calculations of the F/A-18A HARV Inlet Vortex Generators

Steve D. Podleski  
*NYMA, Inc.*  
*Brook Park, Ohio*

November 1995

Prepared for  
Lewis Research Center  
Under Contract NAS3-27186



National Aeronautics and  
Space Administration

## Contents

Summary .....	1
Introduction .....	1
Numerical Modeling .....	2
PARC3D Code .....	2
Grid Geometry .....	2
Boundary Conditions .....	3
Convergence Criteria .....	3
Results .....	4
External Flow Field .....	4
Internal Flow Field .....	5
Conclusions .....	6
Recommendations .....	6
Acknowledgments .....	6
Table I.—PARC3D F/A-18 Grid Block Description .....	7
Appendix A—Symbols .....	8
Appendix B—List of Figures .....	9
Appendix C—PARC3D Input File .....	11
References .....	26



# PARC3D Calculations of the F/A-18A HARV Inlet Vortex Generators

Steve D. Podleski  
NYMA, Inc.  
2001 Aerospace Parkway  
Brook Park, Ohio 44142

## Summary

NASA Lewis Research Center is currently engaged in a research effort as a team member of the High Alpha Technology Program within the NASA agency. This program uses a specially-equipped F/A-18A aircraft called the High Alpha Research Vehicle (HARV), in an effort to improve the maneuverability of high-performance military aircraft at low-subsonic-speed, high-angle-of-attack conditions. The overall objective of the NASA Lewis effort is to develop inlet analysis technology towards efficient airflow delivery to the engine during these maneuvers. One portion of this inlet analysis technology uses computational fluid dynamics to predict installed inlet performance.

Most of the F/A-18A HARV geometry, which includes the ramp/splitter plate, side diverter and slot, inlet lip and upper diverter, and deflected leading-edge flap has been modeled. The empennage and rear fuselage have not. A pair of vortex generators located on the bottom wall of the inlet were not modeled initially. These vortex generators were installed to alleviate any flow separation that may be induced by the wheel well protrusion into the inlet wall. Calculations completed with the PARC3D code showed that the pressure recovery has been underpredicted and the flow distortion overpredicted. To improve the correlation of PARC3D predictions with flight and wind tunnel tests, the vortex generators were included in the grid geometry and the results are presented in this report.

The grid totals 27 blocks or 1.3 million grid points for the half model, which includes the vortex generator grid blocks. Two flight cases were calculated, a high speed case with a Mach number of 0.8 and angle of attack of  $3.4^\circ$ ; and a low speed case with a Mach number of 0.43 and angle of attack of  $32.2^\circ$ . The vortex generators have a significant effect on the inlet boundary layers at high speed, low angle of attack; and have no effect at low speed, high angle of attack.

## Introduction

The purpose of the NASA High Angle of Attack Technology Program is to study the behavior of high performance aircraft at extreme attitudes in order to enhance their effectiveness. One of the main research articles in this program is the F/A-18A HARV (High Angle Research Vehicle) because of its ability to fly extreme flight attitudes (ref. 1). The flight region of most severe engine-inlet distortion occurs at high angles of attack and non-zero sideslip. References 2 and 3 present the results of PARC3D calculations on the F/A-18 HARV at high angles of attack and moderate sideslip angles at various Mach numbers, with emphasis on inlet performance parameters.

The previous PARC3D F/A-18A model did not include a pair of vortex generators located on the bottom wall of the inlet. These vortex generators were installed to prevent flow separation by a wheel well protrusion into the inlet wall. The additional effort to generate a grid for the vortex generators, and the assumption that their small size would not have any significant effect on inlet performance at high angles of attack, contributed to the original decision not to include the vortex generators.

Vortex generators are low-aspect-ratio miniature wings usually installed vertically at critical



areas on exterior surfaces of aircraft experiencing flow separation problems, for example, upstream of ailerons. The low aspect ratio induces strong tip vortices, which mix the high energy flow outside the boundary layer with the low energy flow within the boundary layer. The result, hopefully, delays or prevents flow separation.

The vortex generator study was spurred by the discrepancies between PARC3D calculations and the Northrup flight tests (refs. 4 and 5), and the AEDC wind tunnel tests (ref. 6) of F/A-18 inlet performance. It was thought that the boundary layer mixing effect of the vortex generators would increase pressure recovery and decrease flow distortion at the compressor face, therefore aiding the correlation of PARC3D calculations with test data. An additional purpose of the study was to investigate the capability of the PARC3D code to handle the large difference in geometry and flow scales as represented by the vortex generators inside the inlet.

This report gives a short description of the code, boundary conditions, and grid geometry, followed by a more detailed description of the grids associated with the vortex generators. The presentation of the PARC3D results is split into the external and internal flow fields with emphasis on the latter. The report ends with recommendations and conclusions.

## Numerical Modeling

### PARC3D Code

The PARC3D code (ref. 7) solves the full three-dimensional, Reynolds-averaged, Navier-Stokes equations in strong conservation form using the Beam and Warming approximate factorization scheme to obtain a block tridiagonal system of equations where the domain is decomposed into discrete blocks with block matrix inversion. Pulliam's scalar pentadiagonal transformation provides an efficient solver. The code uses a combination of the Baldwin-Lomax and PD Thomas turbulence models. Trilinear interpolation transfers information between blocks.

### Grid Geometry

Figure 1 and table 1 show the grid block geometry of the complete F/A-18A HARV model and figure 2 shows the surface and plane of symmetry grid point distribution. Including the vortex generators, there are 27 blocks totaling 1.35 million grid points. The grid was generated with the GRIDGEN3D system (ref. 8). The grid density of the lower or windward surfaces are high compared to that of the upper or leeward surfaces of the HARV model; it was assumed that the leeward surfaces would have a secondary influence upon inlet performance. As an indication of grid density, the  $y^+$  values near the corner of the lower surfaces of the LEX (leading edge extension) and fuselage varied between 0.5 and 2.2; the  $y^+$  at the ramp/splitter plate varied between 0.1 and 1.3; the inlet values are between 1.6 and 2.6, whereas the values on the inlet lip are between 0.5 and 2.0. For more details of the grid generation process of the F/A-18A HARV model, see references 9 and 10. Figure 3, a closeup of the inlet region, shows the detail of the geometry in the vicinity of the inlet entry including the ramp/splitter plate, the side diverter and slot, the upper diverter, inlet lip and deflected leading-edge flap. Figure 4 shows the inlet as a contracting and expanding S-duct that makes a transition from a D-shape to a circular cross-section. Figure 5 shows the location and geometry of the vortex generators relative to the inlet. As seen in figure 6, the grid generators are small enough to fall in between the grid lines of the inlet grid. PARC3D requires overlapping grids to transfer flow quantities between block interfaces and the large differential in grid scale would not allow sufficient information to be transferred.



Therefore, this large disparity in geometry scale required a grid denser than the inlet grid to act as an intermediary between the vortex generators and the inlet. This intermediate grid enveloped the vortex generators, their wakes, and trailing vortex sheet.

The axial extent of the intermediate grid extended upstream of the vortex generator by one chord and extended downstream to the compressor face; the azimuthal extent was approximately two chords to one side of one vortex generator and two chords to the other side of the other vortex generator; and the radial extent was near the inlet centerline. The gridding of the vortex generators themselves was split into two blocks; the rectangular span is a "C" grid extending approximately one chord upstream of the leading edge and three chords downstream of the trailing edge; the tip cap is modeled as an "O" grid. Figure 7 shows one grid plane of the inlet, intermediate, and vortex generator grids. Cutouts in the inlet and intermediate grids are also shown. These cutouts increase the number of interfaces between the grid blocks, increasing the interaction between the blocks, and thus lowering the time to solution convergence. Figure 8 is the grid block outline of the vortex generators and intermediate grids, which shows the significant overlap of the vortex generator grids. Figure 9 compares the vortex generator spanwise and inlet radial grid distributions.

Table 1 provides information on the size and type of vortex generator grid. Figure 10 shows the grid indexing convention for the vortex generator grid blocks. For the inlet and intermediate grids, the first index is the axial or downstream direction, and the second index is the circumferential direction, while the third index is the radial direction. The vortex generator span first index is the axial or clockwise direction, the second index is the spanwise direction, and the third index is normal to the span. The vortex generator tip cap first index is the axial/downstream direction, the second index is the circumferential direction, and the third index is normal to the surface. Upstream and downstream of the tip cap, the circumferential index collapses into a pole for the minimum value of the radial index.

During the grid generation process, the root plane of the vortex generator planform was projected onto the inlet wall to minimize any gap. In the actual aircraft, this gap is a mounting plate holding the vortex generators. The spanwise density was high at the root and at the tip. The root density was determined by the boundary layer thickness of the inlet wall; and the tip spacing was influenced by the desired tip vortex definition. The grid density normal to the span wall was relatively sparse, which was done to keep the overall grid size low as it was thought that this would not influence vortex generator performance because the tip vortex is mainly an inviscid phenomenon. The grid density of the intermediate grid is about two to three times denser azimuthally and four to five times denser axially/streamwise than the inlet grid. No changes were made to the grid density normal to the inlet wall.

## Boundary Conditions

Free stream conditions of  $M = 0.8$ , angle of attack of  $3.8^\circ$ , and altitude of 35 000 ft, were used. A constant static pressure was used on the outflow face of the inlet block; its value was determined by iterating to a corrected mass flow of 144 lbs/sec based on a simulated 40-probe rake. Along the windward side of the airframe, no slip, adiabatic wall conditions were used while on the leeward side, inviscid walls were specified. The transfer of flow data between blocks was done with trilinear interpolations. The leading edge flap, inlet lip, and vortex generator grids overlay neighboring grids, and appropriate cutouts of the overlaid grids were made to increase the transfer of flow quantities through the grid interfaces.

Appendix A contains a listing of the NAMELIST and boundary condition input for PARC3D.

## Convergence Criteria

Several convergence criteria were used. The mass flow computed at the fan face was iterated to approximately 1 percent of the desired value; a mass flow ratio near 1 percent to a reference station near



the inlet throat was usually obtained. Another convergence criteria was a change of less than 2 percent in flow distortion and 1 percent in pressure recovery at the fan face between iterations.

In the past, as reported in references 2 and 3, the convergence history of external forces, lift and drag, were monitored. It was found that these forces converged more rapidly than the inlet performance parameters and mass flow. The external forces were not monitored for this study.

The solutions require approximately 120 iterations per hour on the Cray YMP computer. Approximately 10 000 iterations are required towards convergence including 3000 iterations of the whole flow field and another 7000 iterations on the ramp/splitter plate, inlet, lip, upper diverter, and vortex generator grid blocks. The largest block of the F/A-18A HARV PARC3D model requires less than 8 megawords of Cray YMP memory.

## Results

### External Flow Field

Discussions of the external flow field are confined to the windward surfaces of the aircraft because these surfaces would most likely have more influence on inlet performance than the leeward surfaces. Figure 11 shows the simulated surface oil flow as calculated by the FAST graphics program (ref. 11). There are no indications of any major flow separation along the windward aircraft surfaces except near the midpoint of the nacelle, which should not affect inlet performance.

Figure 12 shows the free particle traces as calculated by FAST. The flow is somewhat axial except for a weak vortex generated by the LEX. Figure 12 also shows the flow diverted by the ramp/splitter plate and upper diverter.

Figure 13 shows the restricted particle traces for the case of a high angle of attack. The separation lines on the lower fuselage sides and the attachment line on the lower surface of the LEX are caused by a vortex that is generated by the juncture of these two surfaces. Another separation line is shown on the upper half of the ramp/splitter plate that extends into the inner side wall of the inlet.

Figure 14 shows the unrestricted or free particle traces generated in the case of the high angle of attack. The LEX vortex is generated by the flow over the relatively thin leading edge of the LEX. The LEX-fuselage vortex, as mentioned above, is generated in the corner formed by the lower fuselage and LEX surfaces. This vortex is split by the ramp/splitter plate; a portion of this vortex is directed by the diverter through the LEX slot into the leeward flow. The remainder of the vortex is again split by the upper diverter and the remainder of the vortex is ingested by the inlet.

There is little experimental verification of the flow field patterns as described above. Fisher et al. (ref. 12), completed oil flow studies on the F/A-18A HARV during flight tests but the emphasis was on the external aerodynamics of the leeward surfaces. Figure 15 shows some oil traces that flowed on the windward surface of the fuselage below the LEX apex. The aircraft was flying at an angle of attack of  $26^\circ$  and Mach number near 0.25. This trace seems to indicate a separation line.

Another check on external flow calculations is provided by surface pressure measurements taken by Fisher et al. (ref. 13). Figure 16 shows the fuselage stations along which forebody and LEX surface pressures were taken. Figure 17 compares surface pressure calculations with measurements on five forebody and three LEX stations. The comparisons of the forebody stations are good except for FS 142 which shows two spikes. One spike, at a circumferential angle near  $90^\circ$ , is due to an antenna that is not modeled by the grid. The second spike, at a circumferential angle near  $150^\circ$ , is the footprint of the primary vortex which is not captured by calculations; a previous study (ref. 14) shows that the forebody grid is too sparse to capture this vortex. Comparison of the lower surface pressures of the LEX is good



whereas the comparison of the upper surface is poor. This may be due to insufficient upper surface grid density or to the inviscid flow boundary condition. But the assumption of this study is that the influence of the leeward flow along the upper surfaces is secondary to that on the windward surfaces upstream of the inlet with regard to inlet performance.

## Internal Flow Field

Amin et al. (refs. 4, 5, and 6) measured pressure recovery and flow distortion with 40 pairs of high- and low-frequency response probes on a rake located upstream of the fan face. The rake is an eight-leg, five-ring configuration as shown on figure 18. To simulate the experiments as closely as possible, 40 grid points of the PARC3D grid closest to the probe locations were chosen for the PARC3D calculation of pressure recovery, flow distortion, and mass flow. Incidentally, although out of focus, one can see the vortex generators at the bottom center of figure 18. Figure 19 compares these selected grid points to the full grid.

Figure 20 compares the total pressure contours at the compressor face between flight tests (ref. 4) and PARC3D, with and without vortex generators. The point of view of the observer is aft looking upstream, that is, the aircraft fuselage is on the right of the compressor face representation. The boundary layer is significantly thinned although the effect on the total pressure recovery and flow distortion is small. There is a cross-stream separation at 1 o'clock. The flow distortion measure, D2, is defined as the difference between maximum and minimum total pressure divided by average total pressure at the compressor face.

PARC3D underpredicts pressure recovery and overpredicts flow distortion, and reproduces the total pressure contours fairly well except for some scalloping of the calculated contours. This scalloping may be due to the different contouring programs used by the flight test data reduction program and by the PLOT3D (ref. 15) and FAST graphic packages. Also the PLOT3D/FAST contours used all grid points while the test data is limited to the data from the 40 rake probes. The flap in the PARC3D model was mistakenly deflected and its effect on the solution is unknown.

Figure 21 shows the evolution of the tip vortices off the vortex generators. Figure 21(a) indicates the boundary layer thickness 2.6 chord lengths upstream of the vortex generators' leading edge. Figure 21(b) shows that at 2.2 chord lengths downstream of the vortex generators' trailing edge the tip vortex of one of the vortex generators is much stronger and dominates the flow field for the remainder of the inlet. The rake is located 38 chord lengths downstream of the vortex generators. The rapid dissipation of the vortex may be due to inadequate grid density. Figure 22 shows the evolution of the boundary layer without the presence of vortex generators.

Figure 23 shows the trajectories of particle traces off the tip caps of the vortex generators. The traces terminate near 6 o'clock on the fan face. Notice that the helical pattern dissipates rapidly.

Another set of PARC3D runs were completed at an angle of attack of  $32.2^\circ$  and Mach number of 0.432. This was done to see the effect of the vortex generators at conditions of high angle of attack. Figure 24 compares the total pressure contours and performance data between PARC3D and flight test. Although the extent of the low pressure region is comparable, the orientation of the contours is almost  $90^\circ$  different. No flight tests were done with and without vortex generators installed for these conditions. Comparisons of calculations with and without vortex generators show that there is no significant difference. The extent of flow separation is too great to be influenced by the vortex generators. Figure 25 shows the evolution of the trailing edge vortices off the vortex generators. The vortices are quickly dissipated by the large cross-stream separated boundary layer.

For the high angle of attack case, figure 26 shows that the particle traces off the tips of the vortex generators convect with the separated boundary layer. Figure 27 shows a streamwise cross sectional view of the total pressure contours that cut through one of the vortex generators. The boundary layer is larger



than the span of the vortex generator. Figure 28 can be used as a comparison of the boundary layer thickness in the vicinity of the vortex generators at the high speed, low angle of attack conditions.

## Conclusions

At low angle of attack and low distortion, vortex generators have significant local effects on flow field. PARC3D has the capability to calculate flow details generated by small scale geometries relative to larger scale structures as shown by the results of the effect of vortex generators on the boundary layer that is generated by inlet walls. At high angles of attack and high flow distortions, the vortex generators do not contribute to the reduction of the boundary layer thickness.

## Recommendations

In order to obtain a relatively quick solution with the installed vortex generators, the grid density normal to the surface of the generators was low. It was thought that the boundary layer mixing caused by the trailing sheet of the vortex generator is done mainly by the tip vortex which is an inviscid phenomenon. This grid density should be increased in a follow-up study of the effect of viscosity on vortex generator performance.

The axial/downstream grid density should also be increased to study the effect of grid density of the preservation of the trailing vortex sheet and tip vortex strength, and their effect on boundary layer thickness at the compressor face.

For the high speed case, the flap had been mistakenly deflected on the PARC3D model. Although unpublished calculations for a low speed and low angle of attack case show that the effect on the inlet performance is negligible, this case should be rerun with the flap undeflected.

An effort should be made to model vortex generators mathematically in the PARC3D code. If successful, this will eliminate the effort to generate grids specific to the vortex generators. An intermediate step would be to use the fixed boundary condition offered by PARC to set the flow field generated by two counter-rotating vortices at the desired vertical grid plane in the inlet.

## Acknowledgments

Support of this work by the NASA Lewis Research Center under contract NAS3-27186 is gratefully acknowledged. Interest shown by NASA Project Manager, Thomas Biesiadny, is particularly appreciated. C. Frederic Smith provided helpful suggestions during the work process. Raymond Cosner of McDonnell-Douglas Company supplied the F/A-18A airframe geometry database. In addition, the author thanks Maryann Johnston and Tammy Langhals for their outstanding work in generating the text and figures.



TABLE I.—PARC3D F/A-18 GRID BLOCK DESCRIPTION

Block	Grid index, I × J × K	Grid type	Grid description
1	49 × 41 × 65	O-H	Forebody
2	90 × 33 × 18	O-H	Canopy and upper surface of fuselage and LEX
3	82 × 49 × 50	O-H	Lower surface of fuselage and LEX
4	42 × 49 × 41	O-H	Free stream wrap of blocks 2 and 3
5	34 × 50 × 33	H-H	Side diverter
6	35 × 25 × 42	O-H	Belly next to cowl
7	26 × 58 × 58	O-H	Ramp/splitter plate and lower surface of LEX
8	66 × 50 × 49	O-H	Inlet
9	34 × 26 × 41	H-H	Upper diverter and lower surface of LEX
10	27 × 34 × 34	O-H	Front portion of cowl
11	9 × 41 × 34	O-H	Mid portion of cowl
12	27 × 25 × 18	O-H	Rear portion of cowl and lower fuselage
13	27 × 33 × 18	O-H	Upper fuselage and LEX to the rear of the canopy
14	18 × 25 × 18	O-H	Upper fuselage and LEX to the rear of block 13
15	34 × 57 × 41	O-H	Free stream wrap to the rear of block 4
16	43 × 49 × 26	O-H	Lower surface of wing
17	43 × 33 × 26	O-H	Upper surface of wing
18	11 × 41 × 9	O-H	Free stream wrap of wing block
19	9 × 41 × 33	O-H	Rearmost fuselage block
20	41 × 27 × 33	H-H	Side diverter slot through LEX
21	33 × 37 × 33	C-H	Inlet lip
22	41 × 21 × 26	C-H	Leading-edge flap
23	53 × 27 × 12	C-H	First vortex generator span
24	32 × 21 × 11	O-H	First vortex generator tip cap
25	140 × 16 × 32	O-H	Inlet intermediate grid
26	53 × 27 × 12	C-H	Second vortex generator span
27	32 × 21 × 11	O-H	Second vortex generator tip cap

## Appendix A

### Symbols

$c$	Vortex generator chord length
$C_p$	$(P - P_\infty) / (0.5 \rho_\infty V_\infty^2)$
Corrected Flow Rate	$(m\sqrt{\theta})/\delta$
Distortion, D2	$(P_{Tmax} - P_{Tmin}) / P_{Tavg}$ at compressor face
FS	Fuselage Station in full scale inches (FS = 0 located 60.5 in. ahead of nose)
LEX	Leading edge extension
$m$	Mass flow rate
$P$	Local static pressure
$P_\infty$	Free-stream static pressure
$P_T$	Local total pressure
$P_{Tavg}$	Average total pressure (based on 40-probe rake at compressor face)
$P_{Tmin}$	Minimum total pressure
$P_{Tmax}$	Maximum total pressure
Recovery	Average ratio of $P_T/P_{T\infty}$ from 40-probe rake
$T_{Tavg}$	Average total temperature
$V_\infty$	Free-stream velocity
$\alpha$	Angle of attack
$\beta$	Angle-of-yaw
$x$	Distance from vortex generator
$\delta$	$P_{Tavg} / (14.696 \text{ lb/in.}^2)$
$\rho_\infty$	Free-stream density
$\theta$	$T_{Tavg} / 519.0 \text{ }^\circ\text{R}$ at compressor face



## Appendix B

### List of Figures

1. F/A-18A HARV Grid Block Structure .....	27
2. F/A-18A Surface and Plane of Symmetry Grid .....	28
3. F/A-18A HARV PARC3D Geometry Near Inlet .....	29
4. Isolated Inlet Grid Geometry .....	30
5. Inlet Diffuser and Vortex Generators Schematic .....	31
6. Comparison of Inlet Grid and Vortex Generators .....	32
7. Vortex Generator and Inlet Grid Geometries .....	33
8. Vortex Generator Grid Block Outlines .....	34
9. Vortex Generator Height Relative to Inlet Grid .....	35
10. Grid Block Index Convention .....	36
11. Restricted Particle Traces at $M_\infty = 0.8$ and $\alpha = 3.8^\circ$ .....	37
12. Free Particle Traces at $M_\infty = 0.8$ and $\alpha = 3.8^\circ$ .....	38
13. Restricted Particle Traces at $M_\infty = 0.43$ and $\alpha = 32.2^\circ$ .....	39
14. Free Particle Traces at $M_\infty = 0.43$ and $\alpha = 32.2^\circ$ .....	40
15. Oil Flow Traces from Flight Test at $M_\infty = 0.25$ and $\alpha = 26^\circ$ .....	41
16. Forebody/LEX Surface Pressure Measurement Stations .....	42
17. Surface Pressure Comparisons ( $\alpha = 30^\circ$ and $M_\infty = 0.42$ ) .....	43
18. F/A-18A HARV Engine Face Pressure Measurement Rake .....	44
19. Comparison of PARC3D Grid and Rake .....	44
20. Effect of Vortex Generators on Total Pressure Contours .....	45
21. Evolution of Vortex Generators Total Pressure Contours .....	46
22. Evolution of Total Pressure Contours Without VGs .....	47

23. Particle Traces Off Vortex Generators .....	48
24. Effect of Vortex Generators at High Angle of Attack .....	49
25. Evolution of Total Pressure Contours with VGs .....	50
26. Particle Traces Off Vortex Generators at High Angle of Attack .....	51
27. Cross-Sectional View of Inlet Total Pressure Contours at High Angle of Attack .....	52
28. Cross-Sectional View of Inlet Total Pressure Contours at High Speed .....	53



**Appendix C**  
**PARC3D Input File**

# \$INPUTS

PREF	=	1345.9	NBLOCK	=	27
TREFR	=	501.6	NMAX	=	3000
VRAT	=	-0.6666666667	NC	=	-1
TSUTH	=	0.198600E+03	NSPRT	=	10
RE	=	0.2335E+08	NP	=	3000
PR	=	0.720000E+00	IFXPRT	=	1
PRT	=	0.900000E+00	IFXPLT	=	0
DTCAP	=	0.100000E+02	L2PLOT	=	0
PCQMAX	=	0.100000E+02	IPLOT	=	0
SPLEND	=	0.300000E+00	:LMODE	=	1
SMOO	=	0.000000E+00	MBORD	=	27
STOPL2	=	0.100000E-15	NUMDT	=	0
STOPTR	=	0.500000E+02	IVARDT	=	2
ALPHA	=	32.2	ISOLVE	=	1
BETA	=	0.000000E+00	IRHS	=	1
XMACH	=	0.432	IFILTR	=	2
DDUMP	=	0.100000E+06	IMUTUR	=	3
IFMAX	=	3	NSECTR	=	2
GAMMA	=	0.140000E+01	:LPACK	=	0
DIS2	=	0.240000E+00	:LPRES	=	0
DIS4	=	0.640000E+00	LREST	=	1
			NOBORT	=	0

IBORD=1,2,3,4,5,6,7,21,8,23,24,25,26,27,9,10,11,12,13,14,15,22,16,17,18,19,20

\$END

\*\*\*\*\* 1 front (49, 41, 65)\*\*\*\*\*

\$BLOCK

INVISC(1)=0, INVISC(2)=1, INVISC(3)=1,  
LAMIN(1)=0, LAMIN(2)=1, LAMIN(3)=1,  
NPSEG=1, NBCSEG= 9, DTBLK=10.

\$END

\$PRTSEG

JKLPI(1,1,1)=1,49,10,  
JKLPI(1,2,1)=1,41,10,  
JKLPI(1,3,1)=1,65,10,  
IPORD(1)=3,2,1,

\$END

1	49	1	41	1	1	60	1	0	1.0000	1.0000	30
1	49	1	41	65	65	7	-1	0	0.6291	0.9643	
1	1	2	40	2	64	82	1	0	1.0000	1.0000	
49	49	30	40	2	49	72	-1	6	1.0500	1.0000	
49	49	2	30	2	47	72	-1	7	1.0500	1.0000	
49	49	2	40	2	64	72	-1	8	1.0500	1.0000	
49	49	2	40	2	64	74	-1	8	1.0500	1.0000	
1	49	1	1	2	64	50	1	0	1.0000	1.0000	
1	49	41	41	2	64	50	-1	0	1.0000	1.0000	

\*\*\*\*\* 2 canopy (90, 33, 18)\*\*\*\*\*

\$BLOCK

INVISC(1)=0, INVISC(2)=0, INVISC(3)=0,  
LAMIN(1)=0, LAMIN(2)=0, LAMIN(3)=0,  
NPSEG=1, NBCSEG= 8, DTBLK=4.3

\$END

\$PRTSEG

JKLPI(1,1,1)=1,90,30,  
JKLPI(1,2,1)=1,33,10,  
JKLPI(1,3,1)=1,18,10,  
IPORD(1)=3,2,1,



```

$END
  1  90  1  33  1  1  50  1  0      1.0000  1.0000
  2  46  1  32  18  18  72 -1  10    1.0500  1.0000
45  90  1  32  18  18  72 -1  14    1.0500  1.0000
  2  90  1  32  18  18  74 -1  0     1.0500  1.0000
  1  1  1  32  2  18  71  1  6     1.0500  1.0000
90  90  2  32  2  17  71 -1  16    1.0500  1.0000
  2  90  1  1  2  17  50  1  0     1.0000  1.0000
  1  90  33  33  2  18  50 -1  0     1.0000  1.0000

```

\*\*\*\*\* 3 underlex ( 82, 49, 50)\*\*\*\*\*

```

$BLOCK
  INVISC(1)=1,  INVISC(2)=1,  INVISC(3)=1,
  LAMIN(1)=0,   LAMIN(2)=1,   LAMIN(3)=1,
  NPSEG=1,      NBCSEG= 11,    DTBLK=3.5
  DIS2=0.00

```

\$END

\$PRTSEG

```

  JKLPI(1,1,1)=1,82,10,
  JKLPI(1,2,1)=1,49,10,
  JKLPI(1,3,1)=1,50,10,
  IPORD(1)=3,2,1,

```

```

$END
  1  82  1  48  1  1  60  1  0      1.0000  1.0000  30
  2  48  2  49  50  50  72 -1  9     1.0500  1.0000
46  82  2  49  50  50  72 -1  15    1.0500  1.0000
  2  82  2  49  50  50  74 -1  0     1.0500  1.0000
  1  1  2  49  2  50  71  1  7     1.0500  1.0000
82  82  4  48  2  37  72 -1  18    1.0500  1.0000
82  82  2  7  2  49  72 -1  22    1.0500  1.0000
82  82  4  48  34  49  72 -1  23    1.0500  1.0000
82  82  2  48  2  49  74 -1  0     1.0500  1.0000
  1  82  1  1  2  50  50  1  0     1.0000  1.0000
  2  82  49  49  2  49  60 -1  0     1.0000  1.0000  25

```

\*\*\*\*\* 4 fusmid\_mid ( 42, 49, 41)\*\*\*\*\*

```

$BLOCK
  INVISC(1)=0,  INVISC(2)=0,  INVISC(3)=0,
  LAMIN(1)=0,   LAMIN(2)=0,   LAMIN(3)=0,
  NPSEG=1,      NBCSEG= 8,     DTBLK=6.5

```

\$END

\$PRTSEG

```

  JKLPI(1,1,1)=1,42,10,
  JKLPI(1,2,1)=1,49,10,
  JKLPI(1,3,1)=1,41,10,
  IPORD(1)=3,2,1,

```

```

$END
  2  42  2  36  1  1  72  1  9     1.0500  1.0000
  2  42  34  48  1  1  72  1  10    1.0500  1.0000
  2  42  2  48  1  1  74  1  0     1.0500  1.0000
  1  42  2  48  41  41  7  -1  0     0.6291  0.9643
  1  1  2  48  1  40  71  1  8     1.0500  1.0000
42  42  2  48  2  40  71 -1  13    1.0500  1.0000
  1  42  1  1  1  41  50  1  0     1.0000  1.0000
  1  42  49  49  1  41  50 -1  0     1.0000  1.0000

```

\*\*\*\*\* 5 diverter ( 34, 50, 33)\*\*\*\*\*

```

$BLOCK
  INVISC(1)=1,  INVISC(2)=1,  INVISC(3)=1,
  LAMIN(1)=1,   LAMIN(2)=0,   LAMIN(3)=1,

```

NPSEG=1, NBCSEG= 6, DTBLK=4.  
DIS2=0.00

\$END

\$PRTSEG

JKLPI(1,1,1)=1,34,10,  
JKLPI(1,2,1)=1,50,10,  
JKLPI(1,3,1)=1,33,10,  
IPORD(1)=3,2,1,

\$END

1	33	1	50	1	1	60	1	0	1.0000	1.0000	14
2	33	2	50	33	33	60	-1	0	1.0000	1.0000	20
1	1	2	50	2	33	71	1	18	1.0500	1.0000	
34	34	2	50	2	32	60	-1	0	1.0000	1.0000	15
1	34	1	1	2	33	71	1	21	1.0500	1.0000	
2	33	50	50	2	32	71	-1	20	1.0500	1.0000	

\*\*\*\*\* 6 fuse\_un ( 35, 25, 42)\*\*\*\*\*

\$BLOCK

INVISC(1)=1, INVISC(2)=1, INVISC(3)=1,  
LAMIN(1)=0, LAMIN(2)=1, LAMIN(3)=1,  
NPSEG=1, NBCSEG= 14, DTBLK=20.

\$END

\$PRTSEG

JKLPI(1,1,1)=1,35,10,  
JKLPI(1,2,1)=1,25,10,  
JKLPI(1,3,1)=1,42,10,  
IPORD(1)=3,2,1,

\$END

1	35	1	25	1	1	60	1	0	1.0000	1.0000	22
1	17	2	25	42	42	71	-1	24	1.0500	1.0000	
18	35	2	25	42	42	71	-1	31	1.0500	1.0000	
1	1	2	25	2	41	71	1	22	1.0500	1.0000	
35	35	2	25	2	41	71	-1	34	1.0500	1.0000	
1	35	1	1	2	42	50	1	0	1.0000	1.0000	
34	35	25	25	2	29	50	-1	0	1.0000	1.0000	
2	33	25	25	2	29	72	-1	21	1.0500	1.0000	
2	23	25	25	29	41	72	-1	32	1.0500	1.0000	
21	34	25	25	29	41	72	-1	30	1.0500	1.0000	
2	34	25	25	2	41	74	-1	0	1.0500	1.0000	
2	34	25	25	2	41	73	-1	63	1.0500	1.0000	
2	34	25	25	2	41	73	-1	70	1.0500	1.0000	
2	34	25	25	2	41	73	-1	67	1.0500	1.0000	

\*\*\*\*\* 7 ramp ( 26, 58, 58)\*\*\*\*\*

\$BLOCK

INVISC(1)=1, INVISC(2)=1, INVISC(3)=1,  
LAMIN(1)=0, LAMIN(2)=1, LAMIN(3)=1,  
NPSEG=1, NBCSEG= 16, DTBLK=3.5  
DIS2=0.00

\$END

\$PRTSEG

JKLPI(1,1,1)=1,26,10,  
JKLPI(1,2,1)=1,58,10,  
JKLPI(1,3,1)=1,58,10,  
IPORD(1)=3,2,1,

\$END

2	26	2	57	1	1	60	1	0	1.0000	1.0000	30
1	19	1	58	58	58	72	-1	25	1.0500	1.0000	
16	26	1	58	58	58	72	-1	53	1.0500	1.0000	
1	26	1	58	58	58	72	-1	80	1.05	1.0	



1	26	1	58	58	58	74	-1	0	1.0500	1.0000	
1	1	1	57	1	57	71	1	23	1.0500	1.0000	
26	26	2	57	2	57	72	-1	28	1.2500	1.0000	
26	26	3	21	2	55	72	-1	27	1.2500	1.0000	
26	26	16	57	2	57	72	-1	26	1.2500	1.0000	
26	26	2	57	2	57	72	-1	60	1.2500	1.0000	
26	26	2	57	2	57	74	-1	0	1.0500	1.0000	
26	26	2	57	2	57	73	-1	73	1.0500	1.0000	
26	26	2	57	2	57	73	-1	69	1.0500	1.0000	
2	26	1	1	1	57	71	1	32	1.0500	1.0000	
1	26	58	58	2	57	60	-1	0	1.0000	1.0000	30
						73		2	1.0500	1.0000	

\*\*\*\*\* 8 inlet ( 66, 50, 49)\*\*\*\*\*

\$BLOCK

INVISC(1)=1, INVISC(2)=1, INVISC(3)=1,  
LAMIN(1)=0, LAMIN(2)=1, LAMIN(3)=1,  
NPSEG=1, NBCSEG=29, DTBLK=3.8  
DIS2=0.00

\$END

\$PRTSEG

JKLPI(1,1,1)=66,66,1,  
JKLPI(1,2,1)=1,49,8,  
JKLPI(1,3,1)=1,49,8,  
IPORD(1)=3,2,1,

\$END

15	49	1	50	1	1	60	1	0	1.0000	1.0000	30
49	66	1	8	1	1	60	1	0	1.0000	1.0000	30
49	66	8	50	1	1	60	1	0	1.0000	1.0000	30
2	15	16	34	1	1	60	1	0	1.0000	1.0000	30
2	15	1	16	21	21	71	1	57	1.25	1.25	
2	15	34	50	21	21	71	1	96	1.25	1.25	
1	1	1	48	1	49	72	1	27	1.2500	1.0000	
1	1	1	48	1	49	72	1	61	1.2500	1.0000	
1	1	1	48	1	49	74	1	0	1.0500	1.0000	
1	1	1	50	1	49	71	1	2	1.25	1.0	
15	15	1	16	1	21	71	1	3	1.2500	1.0000	
15	15	34	50	1	21	71	1	4	1.2500	1.0000	
2	15	16	16	2	21	71	1	19	1.25	1.0	
2	15	34	34	2	21	71	-1	17	1.25	1.0	
2	15	1	1	21	48	70	1	5	1.0500	1.0000	
2	15	50	50	21	48	70	-1	5	1.0500	1.0000	
15	65	1	1	2	48	70	1	39	1.0500	1.0000	
15	65	50	50	2	48	70	-1	39	1.0500	1.0000	
						73	1	68	1.0500	1.0000	
						73	1	64	1.0500	1.0000	
						73	1	74	1.0500	1.0000	
2	65	1	50	49	49	82	-1	0	1.0000	1.0000	
66	66	1	8	2	49	0	-1	0	.6025	1.0000	
66	66	11	50	2	49	0	-1	0	.6025	1.0000	
66	66	8	11	30	49	0	-1	0	.6025	1.0000	
49	66	8	8	1	30	71	-1	222	1.0000	1.0000	
49	66	11	11	1	30	71	1	221	1.0000	1.0000	
49	49	8	11	1	30	71	-1	223	1.0000	1.0000	
49	66	8	11	30	30	71	1	224	1.0000	1.0000	

\*\*\*\*\* 9 upper diverter ( 34, 26, 41)\*\*\*\*\*

\$BLOCK

INVISC(1)=1, INVISC(2)=1, INVISC(3)=1,  
LAMIN(1)=0, LAMIN(2)=1, LAMIN(3)=1,

```
NPSEG=1,      NBCSEG= 12,      DTBLK=5.8
DIS2=0.00
```

```
$END
```

```
$PRTSEG
```

```
JKLPI(1,1,1)=1,34,10,
JKLPI(1,2,1)=1,26,10,
JKLPI(1,3,1)=1,41,10,
IPORD(1)=3,2,1,
```

```
$END
```

2	34	2	25	1	1	60	1	0	1.0000	1.0000	16
1	34	2	25	41	41	60	-1	0	1.0000	1.0000	27
1	1	1	26	1	41	72	1	26	1.2500	1.0000	
1	1	2	26	1	23	72	1	59	1.2500	1.0000	
1	1	1	26	1	41	74	1	0	1.0500	1.0000	
1	1	2	26	1	40	73	1	72	1.0500	1.0000	
1	1	2	26	1	40	73	1	65	1.0500	1.0000	
34	34	2	25	2	40	71	-1	38	1.0500	1.0000	
1	27	1	1	1	41	72	1	29	1.0500	1.0000	
25	34	1	1	1	41	72	1	36	1.0500	1.0000	
1	34	1	1	1	41	74	1	0	1.0500	1.0000	
2	34	26	26	2	40	60	-1	0	1.0000	1.0000	14

```
***** 10 cowl_bot+sid( 27, 34, 34)*****
```

```
$BLOCK
```

```
INVISC(1)=1,      INVISC(2)=1,      INVISC(3)=1,
LAMIN(1)=0,      LAMIN(2)=1,      LAMIN(3)=1,
NPSEG=1,      NBCSEG= 12,      DTBLK=8.
DIS2=0.00
```

```
$END
```

```
$PRTSEG
```

```
JKLPI(1,1,1)=1,27,10,
JKLPI(1,2,1)=1,34,10,
JKLPI(1,3,1)=1,34,10,
IPORD(1)=3,2,1,
```

```
$END
```

2	27	2	34	1	1	60	1	0	1.0000	1.0000	23
1	27	1	34	34	34	72	-1	33	1.0500	1.0000	
1	27	1	34	34	34	72	-1	81	1.0500	1.0000	
1	27	1	34	34	34	74	-1	0	1.0500	1.0000	
1	1	1	34	1	33	72	1	28	1.0500	1.0000	
1	1	1	34	1	33	72	1	62	1.0500	1.0000	
1	1	1	34	1	33	74	1	0	1.0500	1.0000	
1	1	1	34	1	33	73	1	66	1.0500	1.0000	
1	1	1	34	1	33	73	1	76	1.0500	1.0000	
27	27	2	34	2	33	71	-1	35	1.0500	1.0000	
1	27	1	1	1	33	71	1	30	1.0500	1.0000	
2	27	34	34	2	33	71	-1	29	1.0500	1.0000	

```
***** 11 cowl_back ( 9, 41, 34)*****
```

```
$BLOCK
```

```
INVISC(1)=1,      INVISC(2)=1,      INVISC(3)=1,
LAMIN(1)=0,      LAMIN(2)=1,      LAMIN(3)=1,
NPSEG=1,      NBCSEG= 11,      DTBLK=17.
```

```
$END
```

```
$PRTSEG
```

```
JKLPI(1,1,1)=1, 9,10,
JKLPI(1,2,1)=1,41,10,
JKLPI(1,3,1)=1,34,10,
IPORD(1)=3,2,1,
```

```
$END
```



1	9	1	41	1	1	60	1	0	1.0000	1.0000	23
2	8	2	41	34	34	72	-1	45	1.0500	1.0000	
2	8	2	41	34	34	72	-1	82	1.0500	1.0000	
2	8	2	41	34	34	74	-1	0	1.0500	1.0000	
1	1	2	12	2	33	72	1	34	1.0500	1.0000	
1	1	7	41	2	33	72	1	35	1.0500	1.0000	
1	1	2	41	2	33	74	1	0	1.0500	1.0000	
9	9	2	41	2	33	71	-1	37	1.0500	1.0000	
2	9	1	1	1	34	50	1	0	1.0000	1.0000	
2	8	41	41	2	33	71	-1	36	1.0500	1.0000	
						73		71			

\*\*\*\*\* 12 midfus ( 27, 25, 18)\*\*\*\*\*

\$BLOCK

INVISC(1)=0, INVISC(2)=0, INVISC(3)=0,  
 LAMIN(1)=0, LAMIN(2)=0, LAMIN(3)=0,  
 NPSEG=1, NBCSEG= 11, DTBLK=10.

\$END

\$PRTSEG

JKLPI(1,1,1)=1,27,10,  
 JKLPI(1,2,1)=1,25,10,  
 JKLPI(1,3,1)=1,18,10,  
 IPORD(1)=3,2,1,

\$END

1	27	1	25	1	1	50	1	0	1.0000	1.0000
1	26	2	25	18	18	72	-1	46	1.0500	1.0000
1	26	2	25	18	18	72	-1	83	1.0500	1.0000
1	26	2	25	18	18	74	-1	0	1.0500	1.0000
1	1	2	24	2	17	72	1	37	1.0500	1.0000
1	1	17	24	2	17	72	1	38	1.0500	1.0000
1	1	2	24	2	17	74	1	0	1.0500	1.0000
27	27	2	25	2	18	71	-1	54	1.0500	1.0000
1	27	1	1	2	18	50	1	0	1.0000	1.0000
1	26	25	25	2	17	50	-1	0	1.0000	1.0000
						73		58	1.0000	1.0000

\*\*\*\*\* 13 fus\_up\_mid1 ( 27, 33, 18)\*\*\*\*\*

\$BLOCK

INVISC(1)=0, INVISC(2)=0, INVISC(3)=0,  
 LAMIN(1)=0, LAMIN(2)=0, LAMIN(3)=0,  
 NPSEG=1, NBCSEG=12, DTBLK=4.5

\$END

\$PRTSEG

JKLPI(1,1,1)=1,27,10,  
 JKLPI(1,2,1)=1,33,10,  
 JKLPI(1,3,1)=1,18,10,  
 IPORD(1)=3,2,1,

\$END

1	27	1	33	1	1	50	1	0	1.0000	1.0000
1	27	1	32	18	18	72	-1	47	1.0500	1.0000
1	27	1	32	18	18	72	-1	84	1.0500	1.0000
1	27	1	32	18	18	74	-1	0	1.0500	1.0000
1	1	2	32	2	17	71	1	16	1.0500	1.0000
27	27	2	32	2	17	71	-1	56	1.0500	1.0000
1	2	1	1	2	17	50	1	0	1.0000	1.0000
3	15	1	1	8	17	50	1	0	1.0000	1.0000
16	27	1	1	2	17	50	1	0	1.0000	1.0000
4	16	1	1	2	7	71	1	52	1.0500	1.0000
1	27	33	33	1	18	50	-1	0	1.0000	1.0000
						73	-1	93	1.0000	1.0000

\*\*\*\*\* 14 fus\_up\_mid2 ( 18, 25, 18)\*\*\*\*\*

\$BLOCK

INVISC(1)=0, INVISC(2)=0, INVISC(3)=0,  
LAMIN(1)=0, LAMIN(2)=0, LAMIN(3)=0,  
NPSEG=1, NBCSEG= 6, DTBLK=5.

\$END

\$PRTSEG

JKLPI(1,1,1)=1,18,10,  
JKLPI(1,2,1)=1,25,10,  
JKLPI(1,3,1)=1,18,10,  
IPORD(1)=3,2,1,

\$END

1	18	1	25	1	1	50	1	0	1.0000	1.0000
1	17	1	24	18	18	71	-1	48	1.0500	1.0000
1	1	2	24	2	17	71	1	56	1.0500	1.0000
18	18	2	24	2	18	71	-1	55	1.0500	1.0000
1	18	1	1	2	17	50	1	0	1.0000	1.0000
1	18	25	25	2	18	50	-1	0	1.0000	1.0000

\*\*\*\*\* 15 bef\_wing\_out( 34, 57, 41)\*\*\*\*\*

\$BLOCK

INVISC(1)=0, INVISC(2)=0, INVISC(3)=0,  
LAMIN(1)=0, LAMIN(2)=0, LAMIN(3)=0,  
NPSEG=1, NBCSEG= 16, DTBLK=5.

\$END

\$PRTSEG

JKLPI(1,1,1)=1,34,10,  
JKLPI(1,2,1)=1,57,10,  
JKLPI(1,3,1)=1,41,10,  
IPORD(1)=3,2,1,

\$END

1	24	2	39	1	1	72	1	15	1.0500	1.0000
1	34	37	56	1	1	72	1	14	1.0500	1.0000
23	34	2	6	1	1	72	1	24	1.0500	1.0000
23	34	5	39	1	1	72	1	25	1.0500	1.0000
1	34	2	56	1	1	72	1	85	1.0500	1.0000
1	34	2	56	1	1	74	1	0	1.0500	1.0000
1	34	2	56	41	41	7	-1	0	0.6291	0.9643
1	1	2	56	2	40	71	1	13	1.0500	1.0000
34	34	37	56	2	36	72	-1	40	1.0500	1.0000
34	34	2	56	33	40	72	-1	41	1.0500	1.0000
34	34	2	39	2	36	72	-1	42	1.0500	1.0000
34	34	2	56	2	40	72	-1	90	1.0500	1.0000
34	34	2	56	2	40	74	-1	0	1.0500	1.0000
1	34	1	1	1	41	50	1	0	1.0000	1.0000
1	34	57	57	1	41	50	-1	0	1.0000	1.0000
						73	-1	88	1.0500	1.0000

\*\*\*\*\* 16 wingbot ( 43, 49, 26)\*\*\*\*\*

\$BLOCK

INVISC(1)=1, INVISC(2)=1, INVISC(3)=1,  
LAMIN(1)=0, LAMIN(2)=1, LAMIN(3)=1,  
NPSEG=1, NBCSEG=22, DTBLK=6.5

\$END

\$PRTSEG

JKLPI(1,1,1)=1,43,10,  
JKLPI(1,2,1)=1,49,10,  
JKLPI(1,3,1)=1,26,10,  
IPORD(1)=3,2,1,



\$END											
1	16	2	7	1	1	72	1	31		1.0500	1.0000
4	16	5	23	1	1	72	1	33		1.0500	1.0000
1	8	5	23	1	1	72	1	53		1.0500	1.0000
14	17	2	23	1	1	72	1	45		1.0500	1.0000
1	17	2	23	1	1	72	1	86		1.0500	1.0000
1	17	2	23	1	1	74	1	0		1.0500	1.0000
18	20	2	48	1	1	72	1	71		1.0500	1.0000
19	42	2	48	1	1	72	1	46		1.0500	1.0000
18	42	2	48	1	1	72	1	75		1.0500	1.0000
18	42	2	48	1	1	74	1	0		1.0500	1.0000
18	42	2	49	26	26	71	-1	43		1.0500	1.0000
2	17	2	24	26	26	71	-1	11		1.0500	1.0000
1	1	2	24	1	26	72	1	42		1.0500	1.0000
1	1	2	24	1	26	72	1	91		1.0500	1.0000
1	1	2	24	1	26	74	1	0		1.0500	1.0000
18	18	25	49	1	26	71	1	77		1.0500	1.0000
43	43	2	49	1	26	71	-1	51		1.0500	1.0000
1	43	1	1	1	26	50	1	0		1.0000	1.0000
18	42	49	49	1	25	60	-1	0		1.0000	1.0000
2	17	24	24	1	25	50	-1	0		1.0000	1.0000
2	17	24	24	1	25	71	-1	78		10.000	1.0000
						73	1	94		1.0500	1.0000

26

\*\*\*\*\* 17 wingup ( 43, 33, 26)\*\*\*\*\*

\$BLOCK

INVISC(1)=0, INVISC(2)=0, INVISC(3)=0,  
 LAMIN(1)=0, LAMIN(2)=0, LAMIN(3)=0,  
 NPSEG=1, NBCSEG= 18, DTBLK=3.5

\$END

\$PRTSEG

JKLPI(1,1,1)=1,43,10,  
 JKLPI(1,2,1)=1,33,10,  
 JKLPI(1,3,1)=1,26,10,  
 IPORD(1)=3,2,1,

\$END											
1	22	8	32	1	1	72	1	47		1.0500	1.0000
1	22	8	32	1	1	72	1	87		1.0500	1.0000
1	22	8	32	1	1	74	1	0		1.0500	1.0000
24	42	2	32	1	1	72	1	48		1.0500	1.0000
23	42	2	32	1	1	72	1	93		1.0500	1.0000
23	42	2	32	1	1	72	1	79		1.0500	1.0000
23	42	2	32	1	1	74	1	0		1.0500	1.0000
2	22	7	32	26	26	71	-1	44		1.0500	1.0000
23	42	1	32	26	26	71	-1	97		1.0500	1.0000
1	1	7	32	1	26	72	1	40		1.0500	1.0000
1	1	7	32	1	26	72	1	92		1.0500	1.0000
1	1	7	32	1	26	74	1	0		1.0500	1.0000
23	23	1	6	1	26	71	1	98		1.05	1.0
43	43	1	32	1	26	71	-1	50		1.0500	1.0000
22	42	1	1	1	25	50	1	0		1.0000	1.0000
2	23	7	7	1	25	71	1	99		1.0000	1.0000
1	43	33	33	1	26	50	-1	0		1.0000	1.0000
						73	1	95		1.0500	1.0000

\*\*\*\*\* 18 wingout ( 11, 41, 9)\*\*\*\*\*

\$BLOCK

INVISC(1)=0, INVISC(2)=0, INVISC(3)=0,  
 LAMIN(1)=0, LAMIN(2)=0, LAMIN(3)=0,  
 NPSEG=1, NBCSEG= 11, DTBLK=15.

\$END

\$PRTSEG

JKLPI(1,1,1)=1,11,10,

JKLPI(1,2,1)=1,41,10,

JKLPI(1,3,1)=1, 9,10,

IPORD(1)=3,2,1,

\$END

1	11	2	28	1	1	72	1	43	1.0500	1.0000
1	11	28	40	1	1	72	1	44	1.0500	1.0000
1	11	2	40	1	1	72	1	89	1.0500	1.0000
1	11	2	40	1	1	74	1	0	1.0500	1.0000
1	11	2	40	9	9	7	-1	0	0.6291	0.9643
1	1	2	40	2	8	71	1	41	1.0500	1.0000
11	11	2	40	2	8	71	-1	49	1.0500	1.0000
1	11	1	1	1	9	50	1	0	1.0000	1.0000
1	11	41	41	1	9	50	-1	0	1.0000	1.0000
						73		97	1.0000	1.0000
						73		11	1.0000	1.0000

\*\*\*\*\* 19 rear ( 9, 41, 33)\*\*\*\*\*

\$BLOCK

INVISC(1)=0, INVISC(2)=0, INVISC(3)=0,

LAMIN(1)=0, LAMIN(2)=0, LAMIN(3)=0,

NPSEG=1, NBCSEG= 11, DTBLK=4.5

\$END

\$PRTSEG

JKLPI(1,1,1)=1, 9,10,

JKLPI(1,2,1)=1,41,10,

JKLPI(1,3,1)=1,33,10,

IPORD(1)=3,2,1,

\$END

1	9	1	41	1	1	50	1	0	1.0000	1.0000
1	8	2	40	33	33	7	-1	0	0.6291	0.9643
1	1	2	40	24	32	72	1	49	1.0500	1.0000
1	1	25	40	2	30	72	1	50	1.0500	1.0000
1	1	2	32	2	30	72	1	51	1.0500	1.0000
1	1	2	32	2	30	72	1	54	1.0500	1.0000
1	1	25	40	2	30	72	1	55	1.0500	1.0000
1	1	2	40	2	32	74	1	0	1.0500	1.0000
9	9	2	40	1	33	0	-1	0	0.6291	1.0000
1	9	1	1	1	33	50	1	0	1.0000	1.0000
1	9	41	41	1	33	50	-1	0	1.0000	1.0000

\*\*\*\*\* 20 slot ( 41, 27, 33)\*\*\*\*\*

\$BLOCK

INVISC(1)=1, INVISC(2)=1, INVISC(3)=1,

LAMIN(1)=1, LAMIN(2)=0, LAMIN(3)=1,

NPSEG=1, NBCSEG= 6, DTBLK=8.5

DIS2=0.00

\$END

\$PRTSEG

JKLPI(1,1,1)=1,41,10,

JKLPI(1,2,1)=1,26,10,

JKLPI(1,3,1)=1,33,10,

IPORD(1)=3,2,1,

\$END

2	40	1	26	1	1	60	1	0	1.0000	1.0000	14
2	40	1	26	33	33	60	-1	0	1.0000	1.0000	20
1	1	2	26	2	32	60	1	0	1.0000	1.0000	15
41	41	1	26	2	32	60	-1	0	1.0000	1.0000	26



1	40	1	1	2	32	71	1	20	1.0500	1.0000
1	41	27	27	1	33	71	-1	52	1.0500	1.0000

\*\*\*\*\* 21 lip ( 33, 37, 33)\*\*\*\*\*

\$BLOCK

INVISC(1)=1, INVISC(2)=1, INVISC(3)=1,  
 LAMIN(1)=0, LAMIN(2)=0, LAMIN(3)=1,  
 NPSEG=1, NBCSEG= 27, DTBLK=7.0  
 DIS2=0.00

\$END

\$PRTSEG

JKLPI(1,1,1)=1,33,10,  
 JKLPI(1,2,1)=1,37,10,  
 JKLPI(1,3,1)=1,33,10,  
 IPORD(1)=3,2,1,

\$END

1	33	1	37	1	1	60	1	0	1.0000	1.0000	22
22	33	25	37	33	33	72	-1	59	1.0500	1.0000	
6	29	1	37	33	33	72	-1	60	1.0500	1.0000	
1	13	1	37	33	33	72	-1	61	1.0500	1.0000	
22	33	1	27	33	33	72	-1	62	1.0500	1.0000	
1	3	20	37	33	33	72	-1	63	1.0500	1.0000	
1	33	1	37	33	33	74	-1	0	1.0500	1.0000	
1	1	1	37	2	32	71	1	64	1.0500	1.0000	
33	33	25	37	2	32	72	-1	65	1.0500	1.0000	
33	33	1	29	2	32	72	-1	66	1.0500	1.0000	
33	33	1	4	2	32	72	-1	67	1.0500	1.0000	
33	33	1	37	2	32	74	-1	0	1.0500	1.0000	
2	19	1	1	2	33	72	1	68	1.0500	1.0000	
7	32	1	1	2	33	72	1	69	1.0500	1.0000	
18	33	1	1	15	33	72	1	70	1.0500	1.0000	
17	32	1	1	2	33	72	1	76	1.0500	1.0000	
2	32	1	1	2	33	74	1	0	1.0500	1.0000	
15	32	37	37	2	32	72	-1	72	1.0500	1.0000	
10	24	37	37	2	32	72	-1	73	1.0500	1.0000	
2	19	37	37	2	32	72	-1	74	1.0500	1.0000	
2	32	37	37	2	32	74	-1	0	1.0500	1.0000	
						73		3	1.0500	1.0000	
						73		4	1.0500	1.0000	
						73		17	1.0500	1.0000	
						73		19	1.0500	1.0000	
						73		57	1.0500	1.0000	
						73		96	1.0500	1.0000	

\*\*\*\*\* 22 flap ( 41, 21, 26)\*\*\*\*\*

\$BLOCK

INVISC(1)=1, INVISC(2)=1, INVISC(3)=1,  
 LAMIN(1)=0, LAMIN(2)=0, LAMIN(3)=1,  
 NPSEG=1, NBCSEG= 29, DTBLK=2.

\$END

\$PRTSEG

JKLPI(1,1,1)=1,41,10,  
 JKLPI(1,2,1)=1,21,10,  
 JKLPI(1,3,1)=1,26,10,  
 IPORD(1)=3,2,1,

\$END

1	41	1	21	1	1	50	1	0	1.0000	1.0000
1	41	1	21	1	1	72	1	80	1.0500	1.0000
1	41	1	21	1	1	72	1	81	1.0500	1.0000
1	41	1	21	1	1	72	1	82	1.0500	1.0000
1	41	1	21	1	1	72	1	83	1.0500	1.0000

1	41	1	21	1	1	72	1	84	1.0500	1.0000
1	41	1	21	1	1	72	1	85	1.0500	1.0000
1	41	1	21	1	1	72	1	86	1.5000	1.0000
1	41	1	21	1	1	72	1	87	1.5000	1.0000
1	41	1	21	1	1	74	1	0	1.0500	1.0000
1	41	1	21	26	26	50	-1	0	1.0000	1.0000
1	41	1	21	26	26	72	-1	88	1.0500	1.0000
1	41	1	21	26	26	72	-1	89	1.0500	1.0000
1	41	1	21	26	26	74	-1	0	1.0500	1.0000
1	41	1	1	1	26	60	1	0	1.0000	1.0000
1	41	21	21	1	26	72	-1	90	1.0500	1.0000
1	41	21	21	1	26	72	-1	91	1.0500	1.0000
1	41	21	21	1	26	72	-1	92	1.0500	1.0000
1	41	21	21	1	26	74	-1	0	1.0500	1.0000
1	1	1	21	1	26	72	1	94	1.0500	1.0000
1	1	1	21	1	26	72	1	58	1.0500	1.0000
1	1	1	21	1	26	74	1	0	1.0500	1.0000
41	41	1	21	1	26	71	-1	95	1.0500	1.0000
						73		79	1.0500	1.0000
						73		98	1.0500	1.0000
						73		99	1.0500	1.0000
						73		77	1.0500	1.0000
						73		78	1.0500	1.0000
						73		75	1.0500	1.0000

\*\*\*\*\* 23 vortex gen 1(53, 27 12)\*\*\*\*\*

\$BLOCK

INVISC(1)=1, INVISC(2)=1, INVISC(3)=1,  
 LAMIN(1)=0, LAMIN(2)=0, LAMIN(3)=1,  
 NPSEG=1, NBCSEG=15, DTBLK=1.5  
 DIS2=0.0

\$END

\$PRTSEG

JKLPI(1,1,1)=1,53,52  
 JKLPI(1,2,1)=1,11,10  
 JKLPI(1,3,1)=1,27,26  
 IPORD(1)=3,2,1,

\$END

1	9	1	1	1	26	-10	1	0	1.0000	1.0000
9	45	1	1	1	26	60	1	0	1.0000	1.0000
45	53	1	1	1	26	5	1	0	1.0000	1.0000
1	53	11	11	1	26	72	-1	204	1.0000	1.0000
1	53	11	11	1	26	72	-1	225	1.0000	1.0000
1	53	11	11	1	26	74	-1		1.0000	1.0000
53	53	1	11	1	26	71	-1	206	1.25	1.25
1	1	1	11	1	26	71	1	210	1.25	1.25
1	53	2	11	1	1	60	1	0	1.000	1.0000
1	53	1	11	27	27	71	-1	214	1.000	1.0000
1	53	1	11	27	27	71	-1	216	1.000	1.0000
						73		208	1.000	1.0000
						73		212	1.000	1.0000
						73		215	1.000	1.0000
						73		247	1.000	1.0000

\*\*\*\*\* 24 vortex gen 1 tip(32, 21, 11)\*\*\*\*\*

\$BLOCK

INVISC(1)=1, INVISC(2)=1, INVISC(3)=1,  
 LAMIN(1)=0, LAMIN(2)=0, LAMIN(3)=0,  
 NPSEG=1, NBCSEG=13, DTBLK=8.  
 DIS2=0.0



\$END

\$PRTSEG

JKLPI(1,1,1)=1,32,31

JKLPI(1,2,1)=1,21,20

JKLPI(1,3,1)=1,11,10

IPORD(1)=3,2,1,

\$END

1	4	1	21	1	1	82	1	0	1.0000	1.0000
25	32	1	21	1	1	82	1	0	1.0000	1.0000
5	24	1	21	1	1	60	1	0	1.0000	1.0000
1	32	1	21	11	11	71	-1	209	1.0000	1.0000
1	1	1	21	1	11	71	1	205	1.0000	1.0000
32	32	1	21	1	11	71	-1	207	1.0000	1.0000
1	32	1	1	1	11	71	1	214	1.0000	1.0000
1	32	21	21	1	11	72	-1	215	1.0000	1.0000
1	32	21	21	1	11	72	-1	249	1.0000	1.0000
1	32	21	21	1	11	74	-1		1.0000	1.0000
1	32	1	1	1	11	71	1	213	1.0000	1.0000
1	32	21	21	1	11	71	-1	211	1.0000	1.0000
						73		248		

\*\*\*\*\* 25 inlet\_slice (140, 16, 32)\*\*\*\*\*

\$BLOCK

INVISC(1)=1, INVISC(2)=1, INVISC(3)=1,  
LAMIN(1)=0, LAMIN(2)=1, LAMIN(3)=1,  
NPSEG=1, NBCSEG=36, DTBLK=5.5  
DIS2=0.00

\$END

\$PRTSEG

JKLPI(1,1,1)=1,140,139

JKLPI(1,2,1)=1,16,15

JKLPI(1,3,1)=1,32,30

IPORD(1)=3,2,1,

\$END

1	9	1	16	1	1	60	1	0	1.00	1.00	30
16	140	1	16	1	1	60	1	0	1.00	1.00	30
9	16	1	8	1	1	60	1	0	1.00	1.00	30
9	16	10	16	1	1	60	1	0	1.00	1.00	30
1	140	1	16	32	32	71	-1	224	1.25	1.25	
140	140	1	16	2	32	0	-1	0	.6025	1.00	
1	1	1	16	2	32	71	1	223	1.25	1.00	
2	139	1	1	2	32	71	1	222	1.25	1.25	
2	139	16	16	2	32	71	-1	221	1.25	1.25	
9	9	6	10	2	28	72	-1	204	1.25	1.25	
9	9	6	10	2	28	72	-1	205	1.25	1.25	
9	9	6	10	2	28	72	-1	226	1.25	1.25	
9	9	6	10	2	28	72	-1	227	1.25	1.25	
9	9	6	10	2	28	74	-1		1.25	1.25	
16	16	6	10	2	28	72	1	206	1.25	1.25	
16	16	6	10	2	28	72	1	207	1.25	1.25	
16	16	6	10	2	28	72	1	228	1.25	1.25	
16	16	6	10	2	28	72	1	229	1.25	1.25	
16	16	6	10	2	28	74	1		1.25	1.25	
9	16	6	10	28	28	72	1	208	1.25	1.25	
9	16	6	10	28	28	72	1	209	1.25	1.25	
9	16	6	10	28	28	72	1	230	1.25	1.25	
9	16	6	10	28	28	72	1	231	1.25	1.25	
9	16	6	10	28	28	74	1		1.25	1.25	
9	16	6	6	2	28	72	-1	210	1.25	1.25	
9	16	6	6	2	28	72	-1	211	1.25	1.25	

9	16	6	6	2	28	72	-1	232	1.25	1.25
9	16	6	6	2	28	72	-1	233	1.25	1.25
9	16	6	6	2	28	74	-1		1.25	1.25
9	16	10	10	2	28	72	1	212	1.25	1.25
9	16	10	10	2	28	72	1	213	1.25	1.25
9	16	10	10	2	28	72	1	234	1.25	1.25
9	16	10	10	2	28	72	1	235	1.25	1.25
9	16	10	10	2	28	74	1		1.25	1.25
						73		216		
						73		238		

\*\*\*\*\* 26 vortex gen 2(53, 27 12)\*\*\*\*\*

\$BLOCK

INVISC(1)=1, INVISC(2)=1, INVISC(3)=1,  
 LAMIN(1)=0, LAMIN(2)=0, LAMIN(3)=1,  
 NPSEG=1, NBCSEG=15, DTBLK=1.  
 DIS2=0.0

\$END

\$PRTSEG

JKLPI(1,1,1)=1,53,52  
 JKLPI(1,2,1)=1,11,10  
 JKLPI(1,3,1)=1,27,26  
 IPORD(1)=3,2,1,

\$END

1	9	1	1	1	26	-10	1	0	1.0000	1.0000
9	45	1	1	1	26	60	1	0	1.0000	1.0000
45	53	1	1	1	26	5	1	0	1.0000	1.0000
1	53	11	11	1	26	72	-1	226	1.0000	1.0000
1	53	11	11	1	26	72	-1	247	1.0000	1.0000
1	53	11	11	1	26	74	-1		1.0000	1.0000
53	53	1	11	1	26	71	-1	228	1.25	1.25
1	1	1	11	1	26	71	1	232	1.25	1.25
1	53	2	11	1	1	60	1	0	1.000	1.0000
1	53	1	11	27	27	71	-1	236	1.000	1.0000
1	53	1	11	27	27	71	-1	238	1.000	1.0000
						73		230	1.000	1.0000
						73		234	1.000	1.0000
						73		237	1.000	1.0000
						73		225	1.000	1.0000

\*\*\*\*\* 27 vortex gen 2 tip(32, 21, 11)\*\*\*\*\*

\$BLOCK

INVISC(1)=1, INVISC(2)=1, INVISC(3)=1,  
 LAMIN(1)=0, LAMIN(2)=0, LAMIN(3)=0,  
 NPSEG=1, NBCSEG=13, DTBLK=9.  
 DIS2=0.0

\$END

\$PRTSEG

JKLPI(1,1,1)=1,32,31  
 JKLPI(1,2,1)=1,21,20  
 JKLPI(1,3,1)=1,11,10  
 IPORD(1)=3,2,1,

\$END

1	4	1	21	1	1	82	1	0	1.0000	1.0000
25	32	1	21	1	1	82	1	0	1.0000	1.0000
5	24	1	21	1	1	60	1	0	1.0000	1.0000
1	32	1	21	11	11	71	-1	231	1.0000	1.0000
1	1	1	21	1	11	71	1	227	1.0000	1.0000
32	32	1	21	1	11	71	-1	229	1.0000	1.0000



1	32	1	1	1	11	71	1	236	1.0000	1.0000
1	32	21	21	1	11	72	-1	237	1.0000	1.0000
1	32	21	21	1	11	72	-1	248	1.0000	1.0000
1	32	21	21	1	11	74	-1		1.0000	1.0000
1	32	1	1	1	11	71	1	235	1.0000	1.0000
1	32	21	21	1	11	71	-1	233	1.0000	1.0000
						73		249	1.000	1.0000

## References

1. Bowers, A.H.; Regenie, V.A.; and Flick, B.C.: F-18 High Alpha Research Vehicle. Fourth High Alpha Conference, NASA Dryden Flight Research Center, 1994.
2. Podleski, S.D.: F/A-18 Inlet Calculations at 60-Deg Angle of Attack and 10-Deg Sideslip. J. of Propulsion and Power, vol. 10, no. 6, pp. 848-854.
3. Podleski, S.D.: Installed F/A-18 Inlet Flow Calculations at High Angles of Attack and Moderate Sideslip. Fourth High Alpha Conference, NASA Dryden Flight Research Center, vol. 2, 1994 (also NASA CP-10143, 1994).
4. Amin, N.F.; and Hollwenger, D.J.: F/A-18 Inlet/Engine Compatibility Test Results. J. of Aircraft, vol. 20, no. 8, 1983.
5. Amin, A.F.; Richards, C.J.; de la Vega, E.G.; and Dhanidina, M.A.: F/A-18A Engine Inlet Survey Report, vols. 1, 2, and 3. NOR 81-3161, Northrop Corporation, Aircraft Division, Hawthorne, CA, Nov. 1981.
6. Amin, A.F.; Franks, W.J.; de la Vega, E.G.; Yamada, M.; Hollweger, D.J.; and Tsukahira, T.W.: AEDC Series 1 F-18 .192 Scale Inlet Test Analysis Report. NOR 77-310, Northrop Corporation, Aircraft Division, Hawthorne, CA, May 1977.
7. Cooper, G.K.; and Sirbaugh, J.R.: PARC Code: Theory and Usage. AEDC-TR-89-15, Dec. 1989.
8. Steinbrenner, J.P.; Chawner, J.R.; and Fouts, C.L.: The GRIDGEN 3D Multiple Block Grid Generation System, Vol II: User's Manual. Wright Research and Development Center, WRDC-TR-90-3022, vol. II, July 1990.
9. Bruns, J.E.; and Smith, C.F.: Full Navier-Stokes Calculations on the F/A-18 Inlet at a High Angle-of-Attack. AIAA/SAE/ASME/ASEE 28th Joint Propulsion Conference and Exhibit, July 6-8, 1992, Nashville, TN.
10. Smith, C.F.; and Podleski, S.D.: Installed F/A-18 Inlet Flow Calculations at 30 Deg. Angle-of-Attack: A Comparative Study. NASA CR-195297, 1994.
11. Walatka, P.M.; Clucas, J.C.; McCabe, R.K.; Plessel, T.; and Potter, R.: FAST User Guide. June 1993.
12. Fisher, D.F.; Del Frate, J.H.; and Richwine, D.M.: In-Flight Flow Visualization Characteristics of the NASA F-18 High Alpha Research Vehicle at High Angles of Attack. NASA TM-4193, 1990.
13. Fisher, D.F.; Banks, D.W.; and Richwine, D.M.: F-18 High Alpha Research Vehicle Surface Pressures: Initial In-Flight Results and Correlation with Flow Visualization and Wind-Tunnel Data. NASA TM-101724, 1990.
14. Smith, C.F.; and Podleski, S.D.: Thin Layer and Full Navier-Stokes Calculations for Turbulent Supersonic Flop Over a Nose Cone at an Angle-of-Attack. NASA CR-189103, 1993.
15. Walatka, P.M.; Buning, P.G.; Pierce, L.; and Elson, P.: PLOT3D User. NASA TM-101067, 1992.



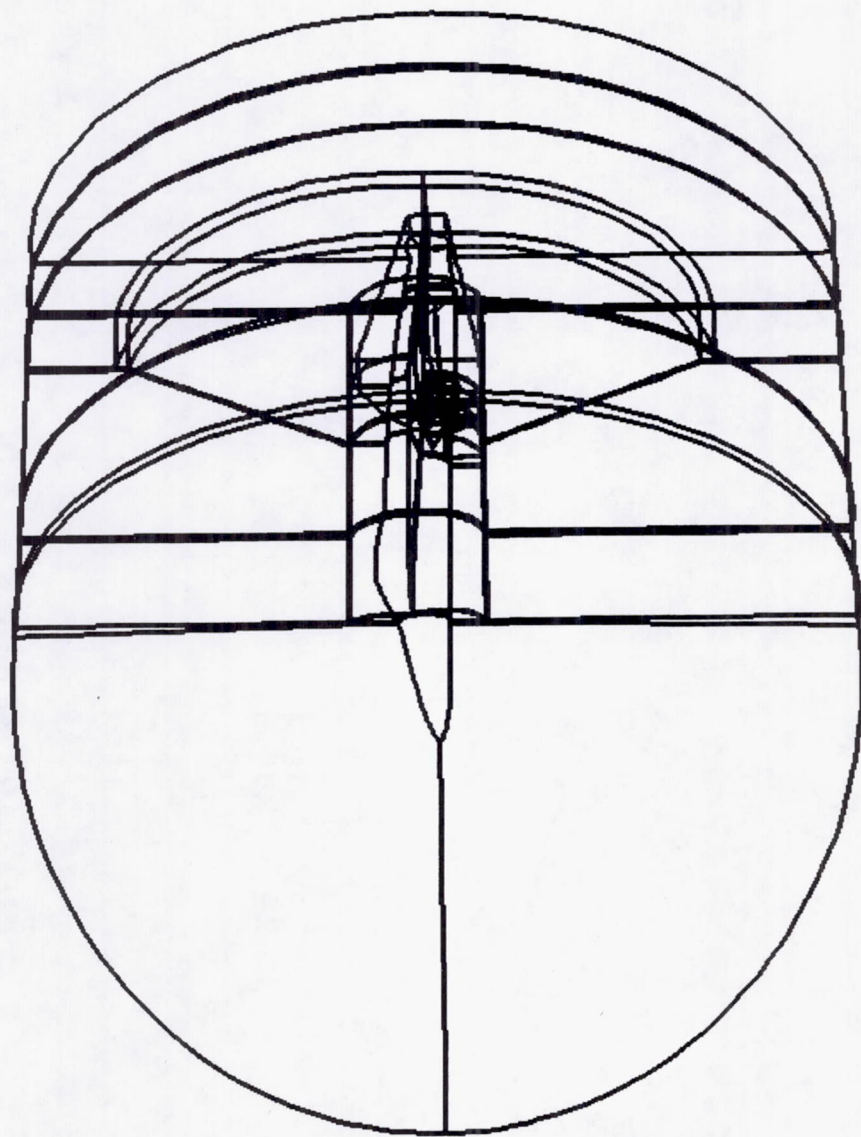


**Fig. 1 - F/A-18A Grid Block Structure**

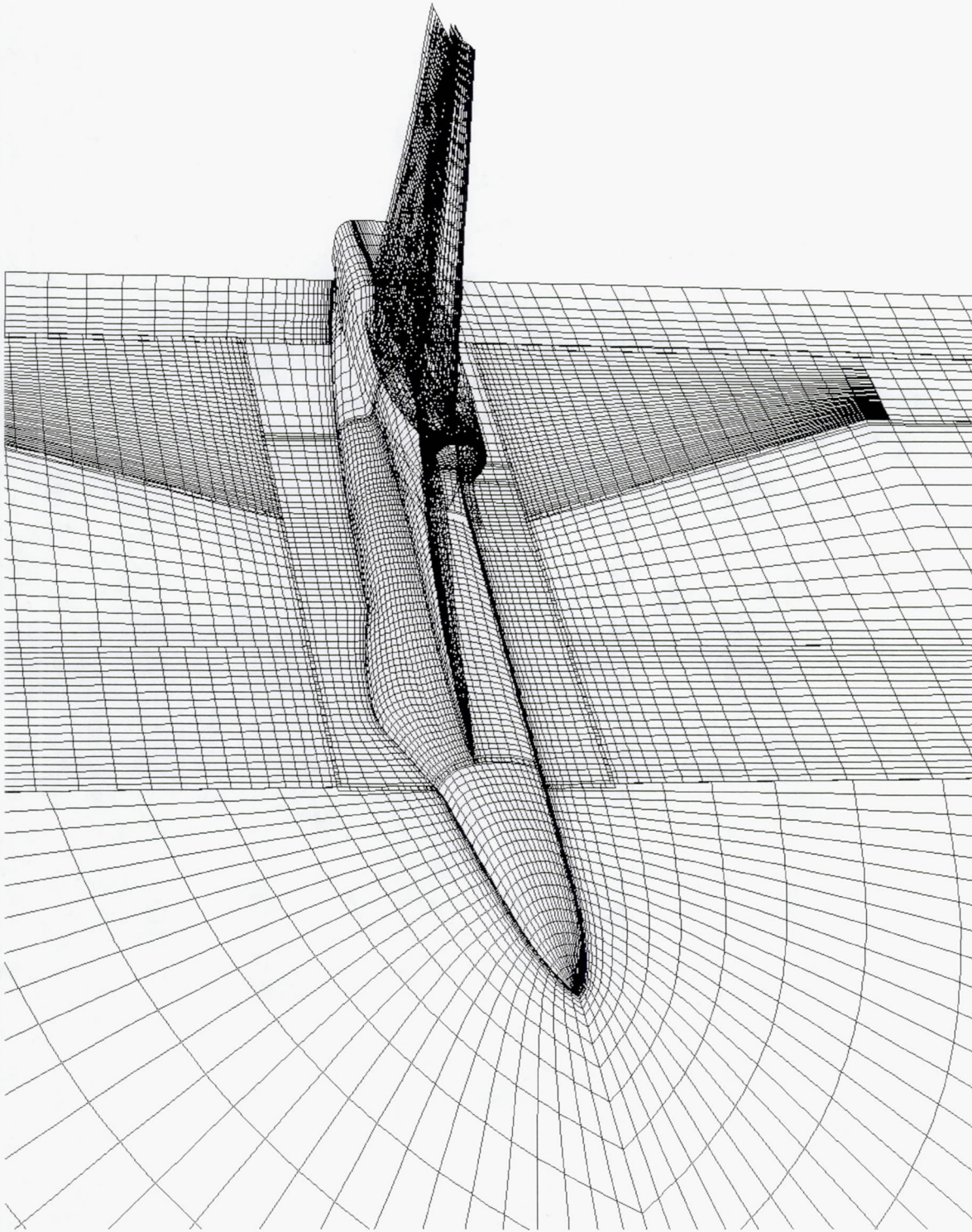


**Fig. 2 - F/A-18A Surface and Plane of Symmetry Grid**



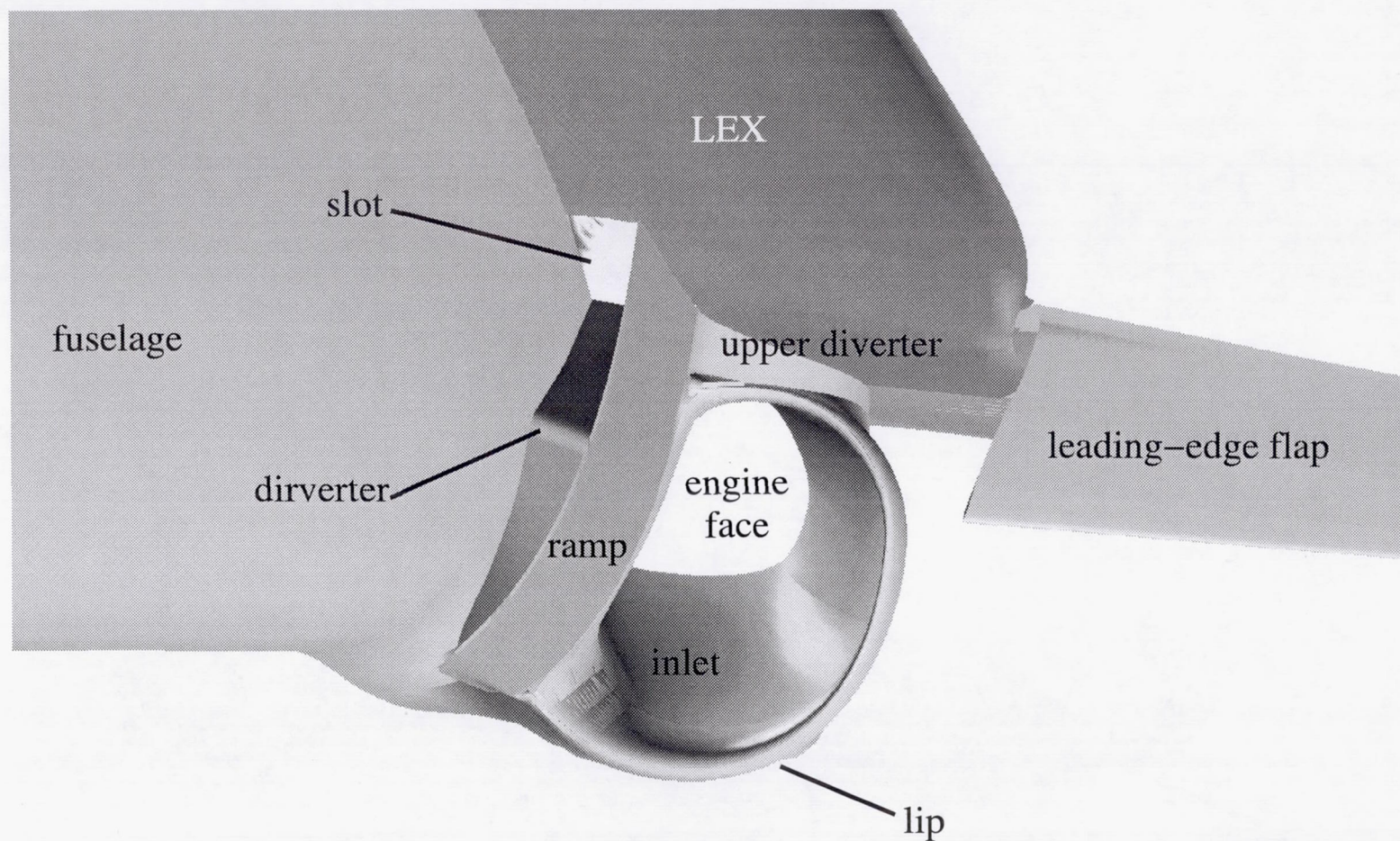


**Fig. 3 – F/A-18A HARV PARC3D Geometry Near Inlet**



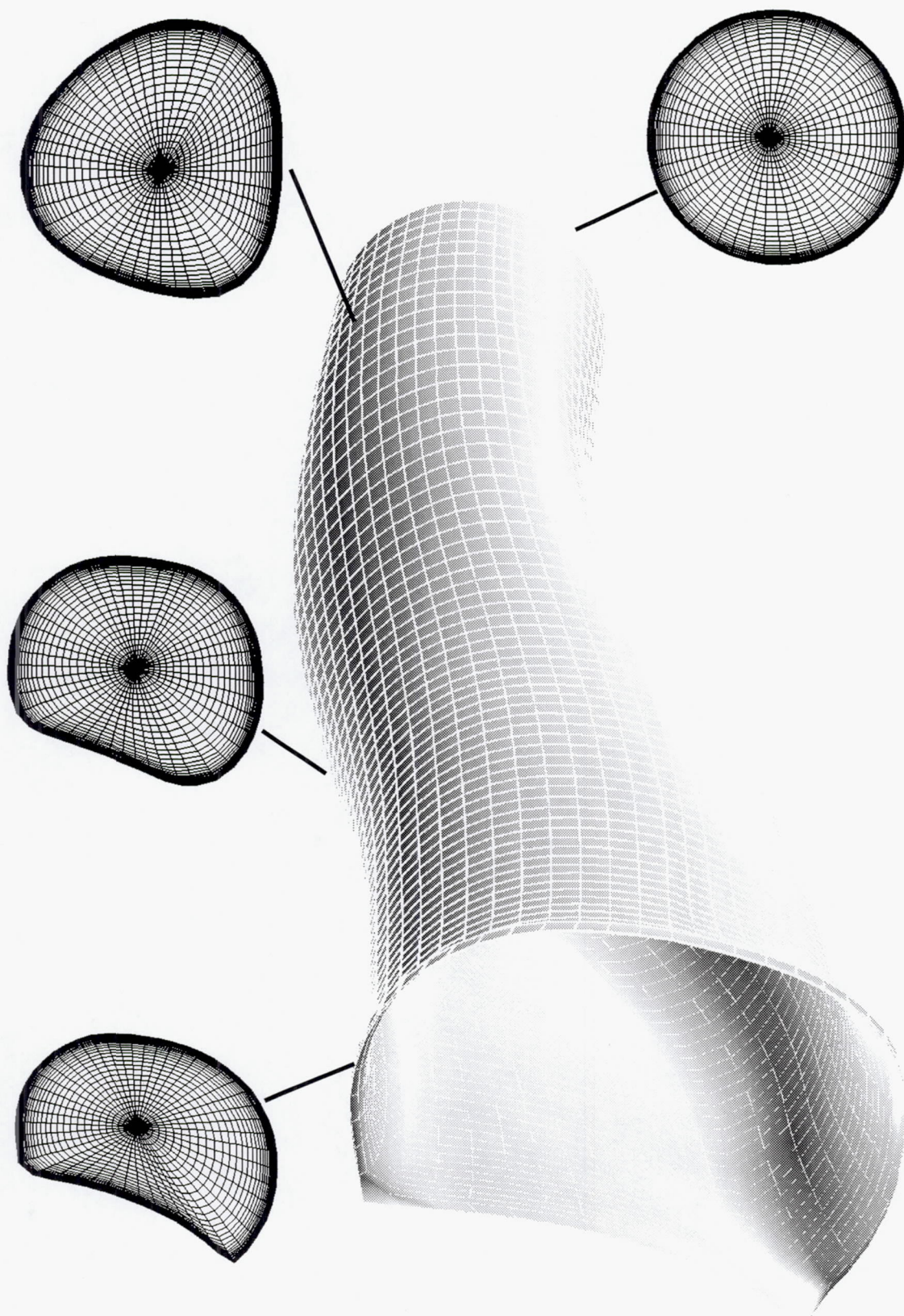


**Fig. 4 – Isolated Inlet Grid Geometry**



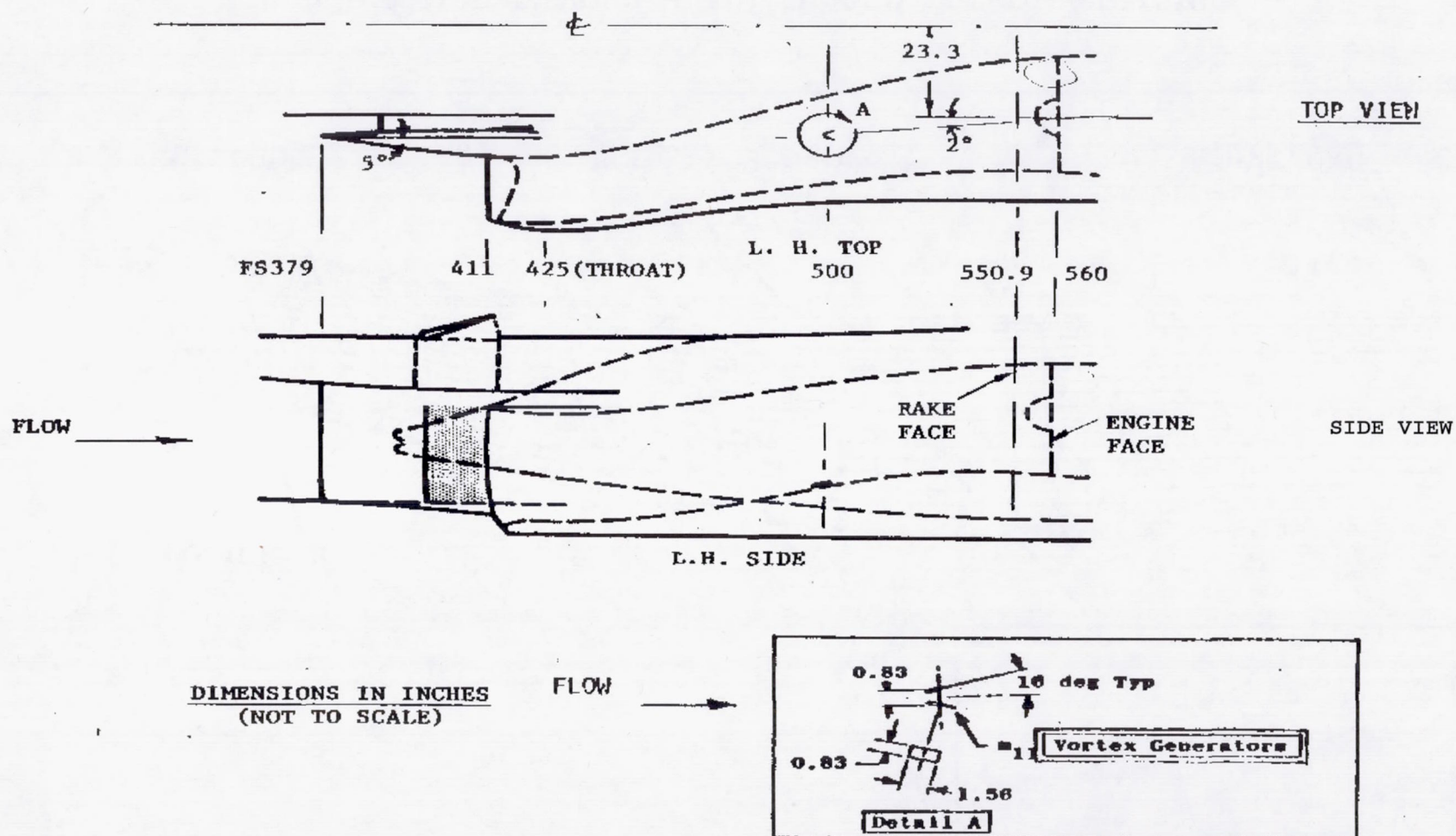


**Fig. 5 – Inlet Diffuser and Vortex Generators Schematic**

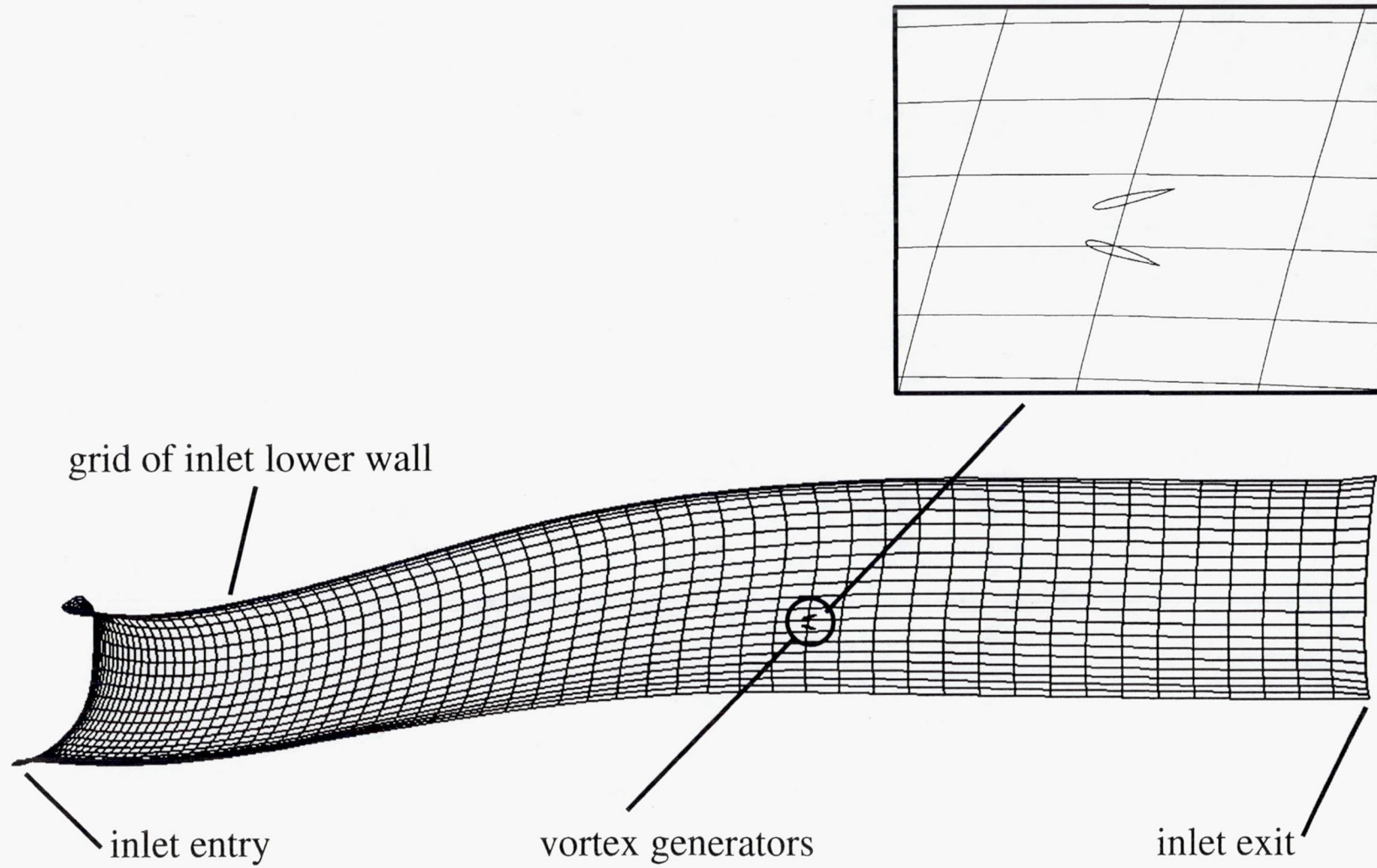


**Fig. 6 – Comparison of Inlet Grid and Vortex Generators**



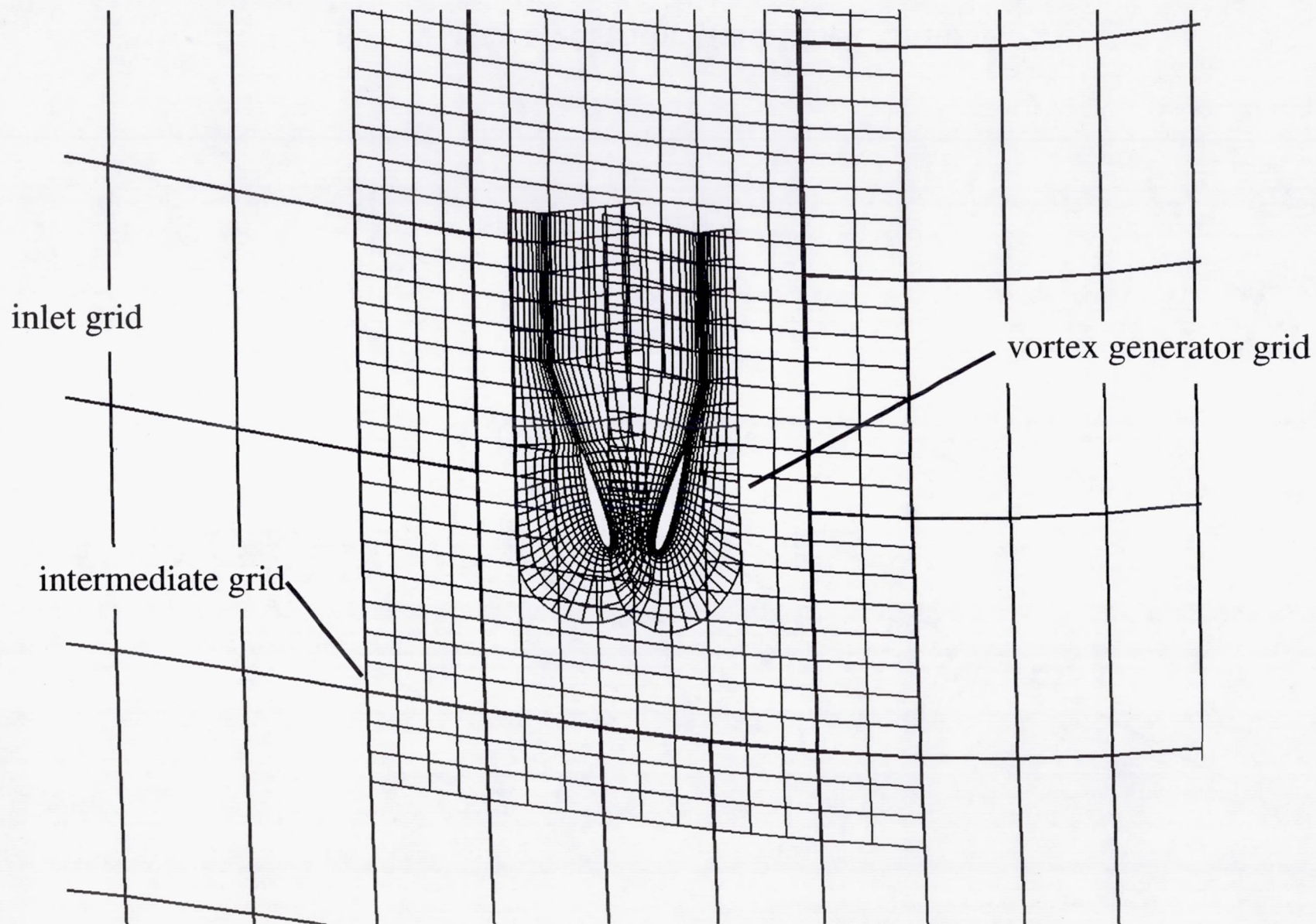


**Fig. 7 – Vortex Generator and Inlet Grid Geometries**

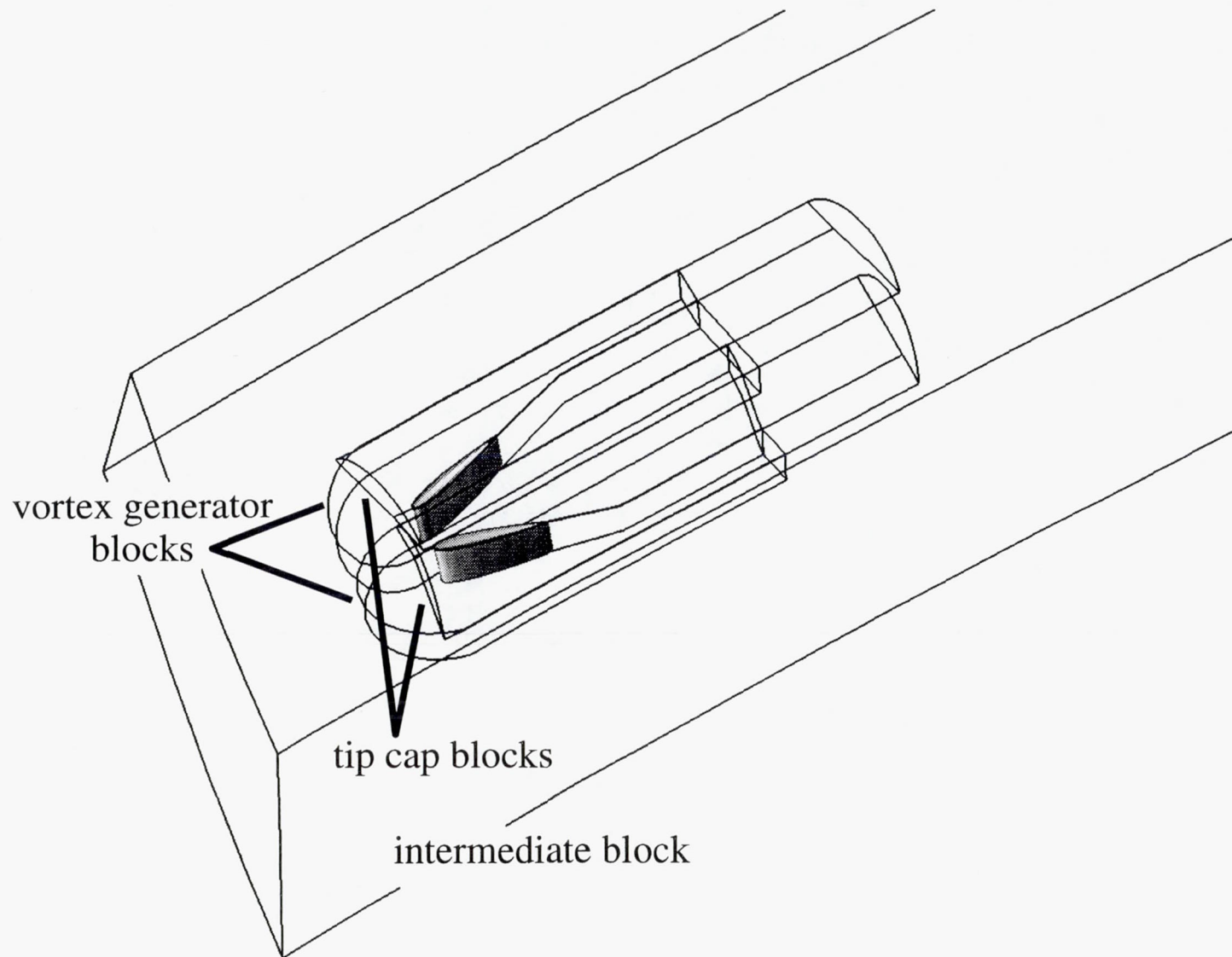


**Fig. 8 – Vortex Generator Grid Block Outlines**



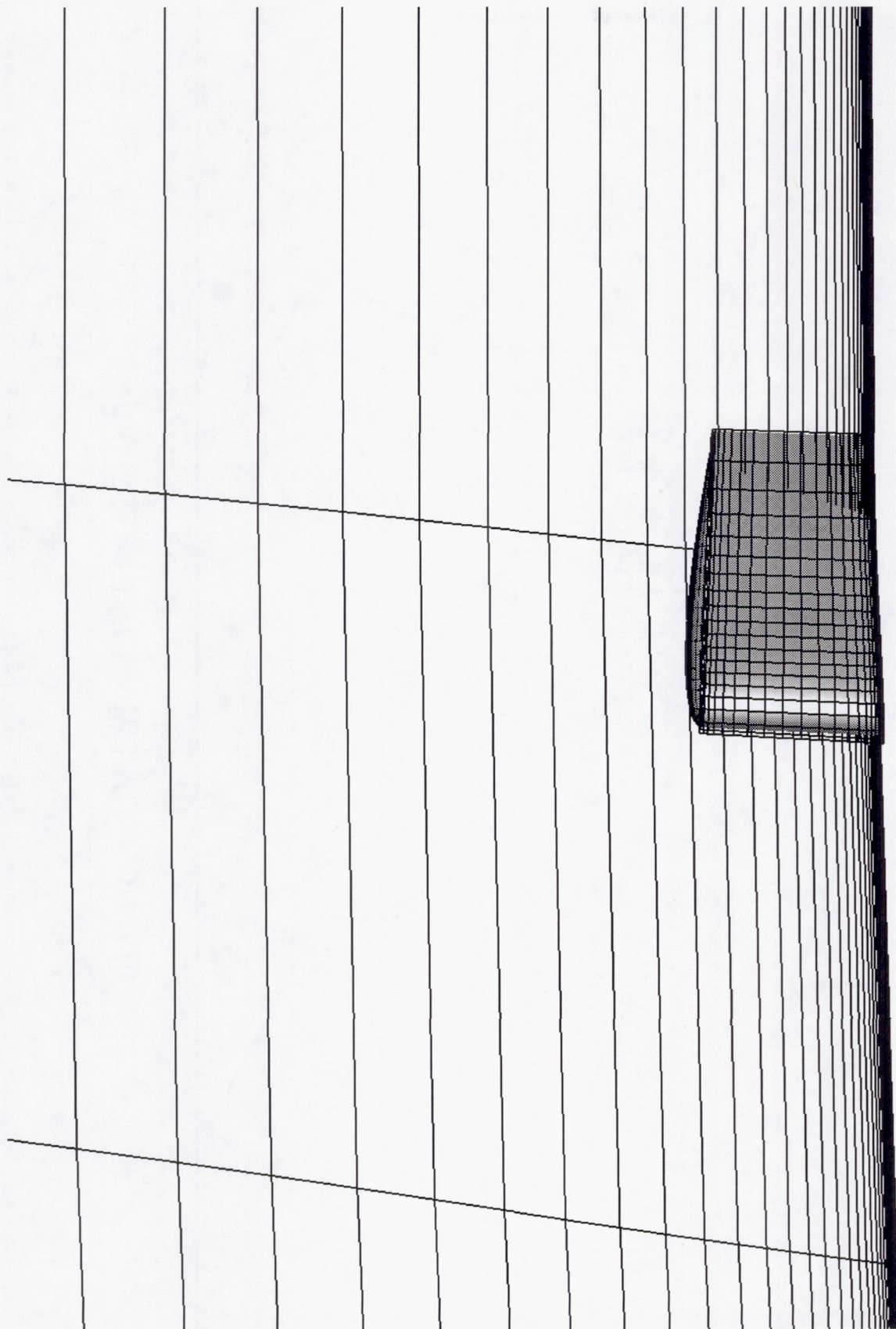


**Fig. 9 – Vortex Generator Height Relative to Inlet Grid**

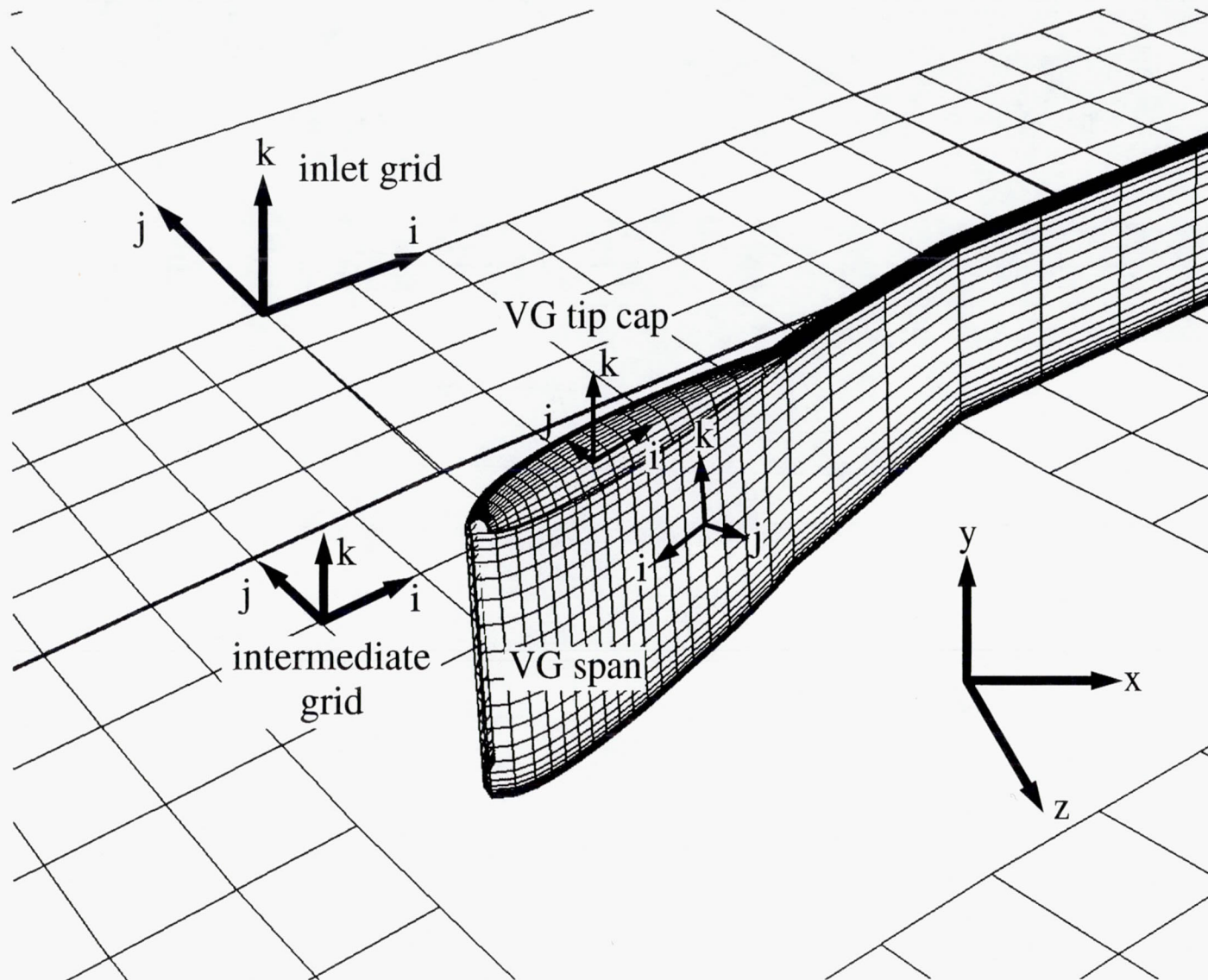


**Fig. 10 – Grid Block Index Convention**



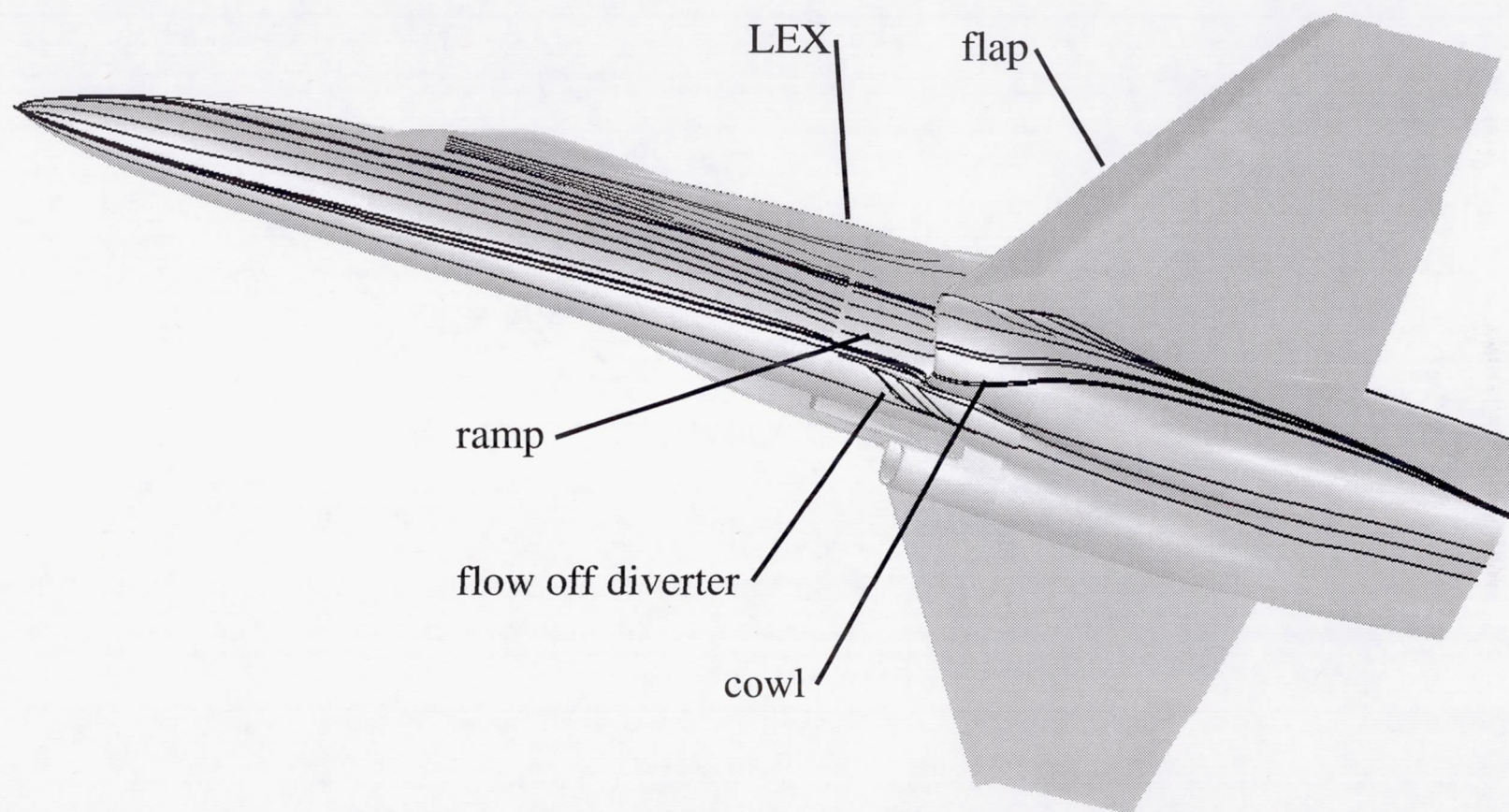


**Fig. 11 – Restricted Particle Traces at  $M_\infty = 0.8$  and  $\alpha = 3.8^\circ$**

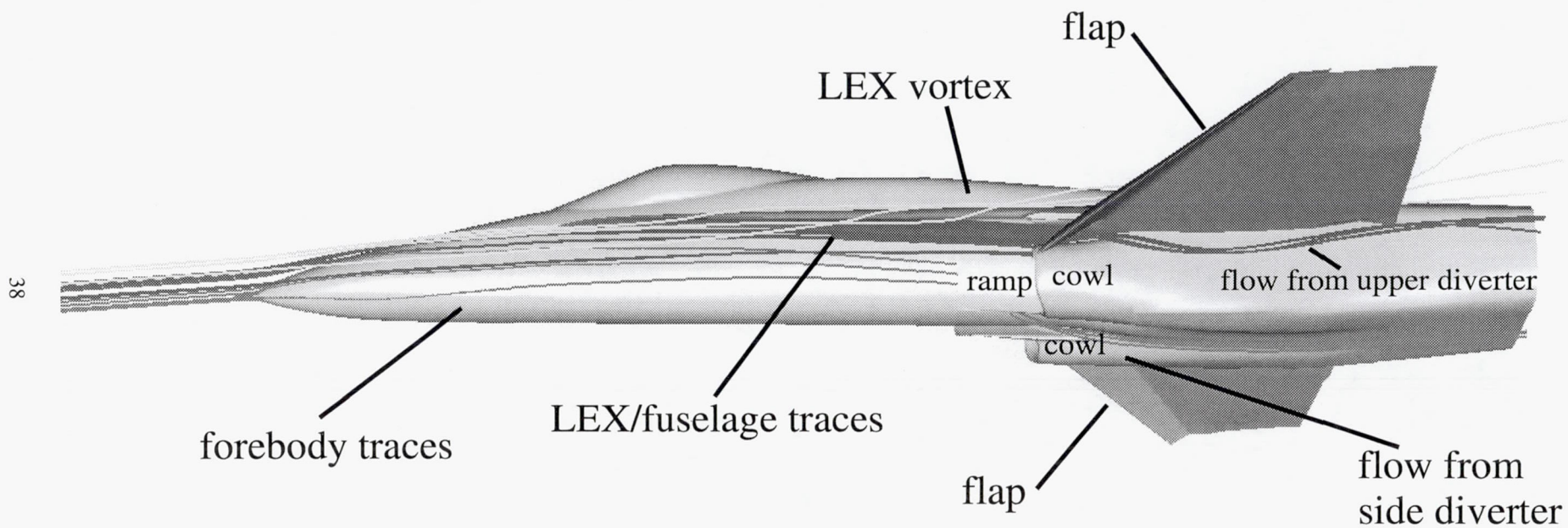


**Fig. 12 – Free Particle Traces  $M_\infty = 0.8$  and  $\alpha = 3.8^\circ$**



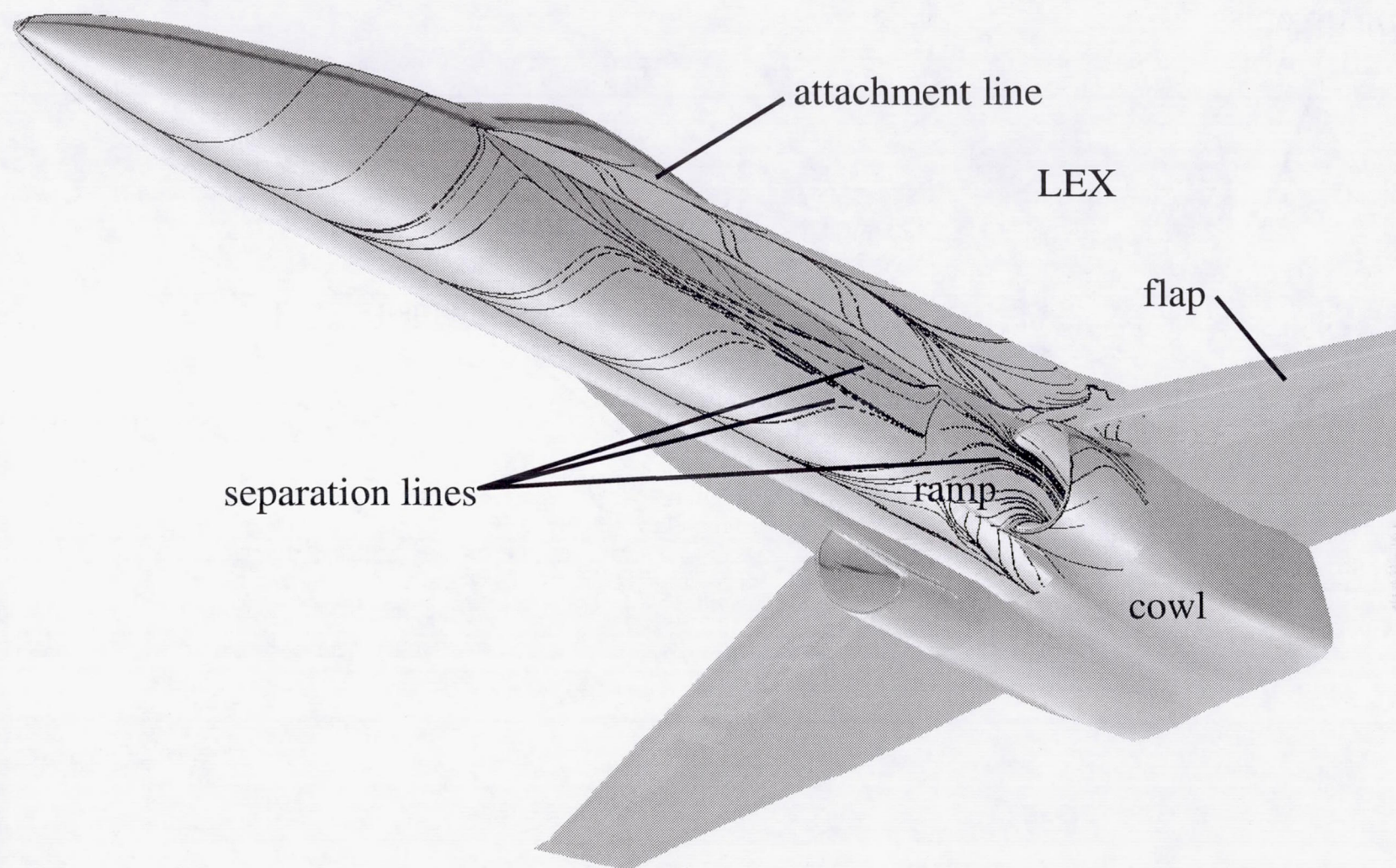


**Fig. 13 – Restricted Particle Traces  $M_\infty = 0.43$  and  $\alpha = 32.2^\circ$**



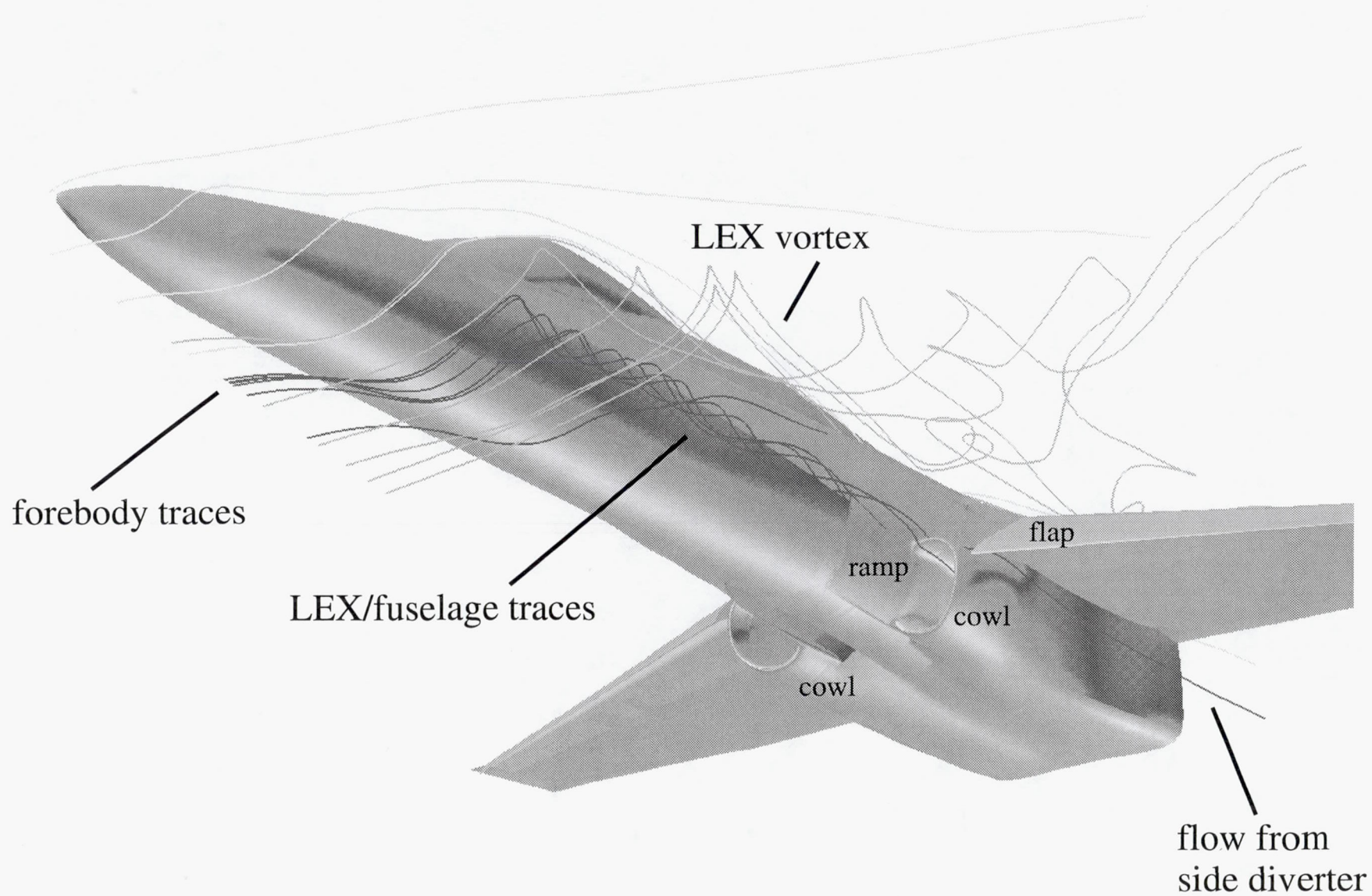


**Fig. 14 – Free Particle Traces at  $M_\infty = 0.43$  and  $\alpha = 32.2^\circ$**



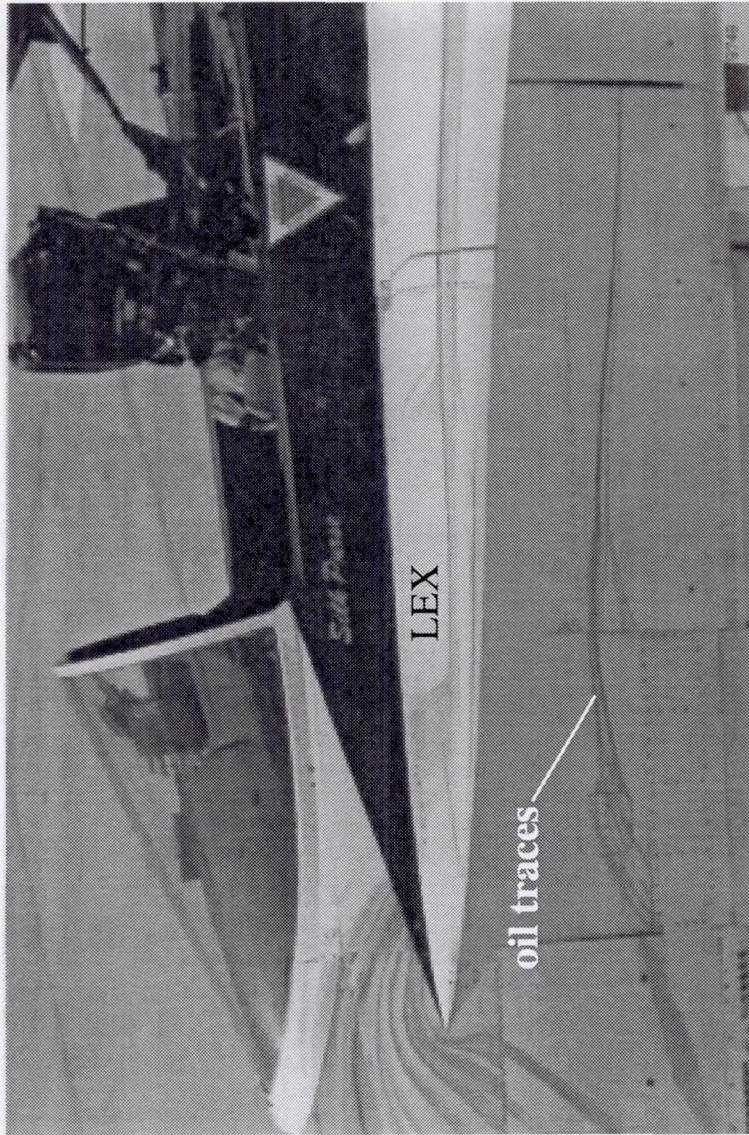


**Fig. 15 – Oil Flow Traces from Flight Test at  $M_{\infty} = 0.25$ ,  $\alpha = 26.0^{\circ}$**

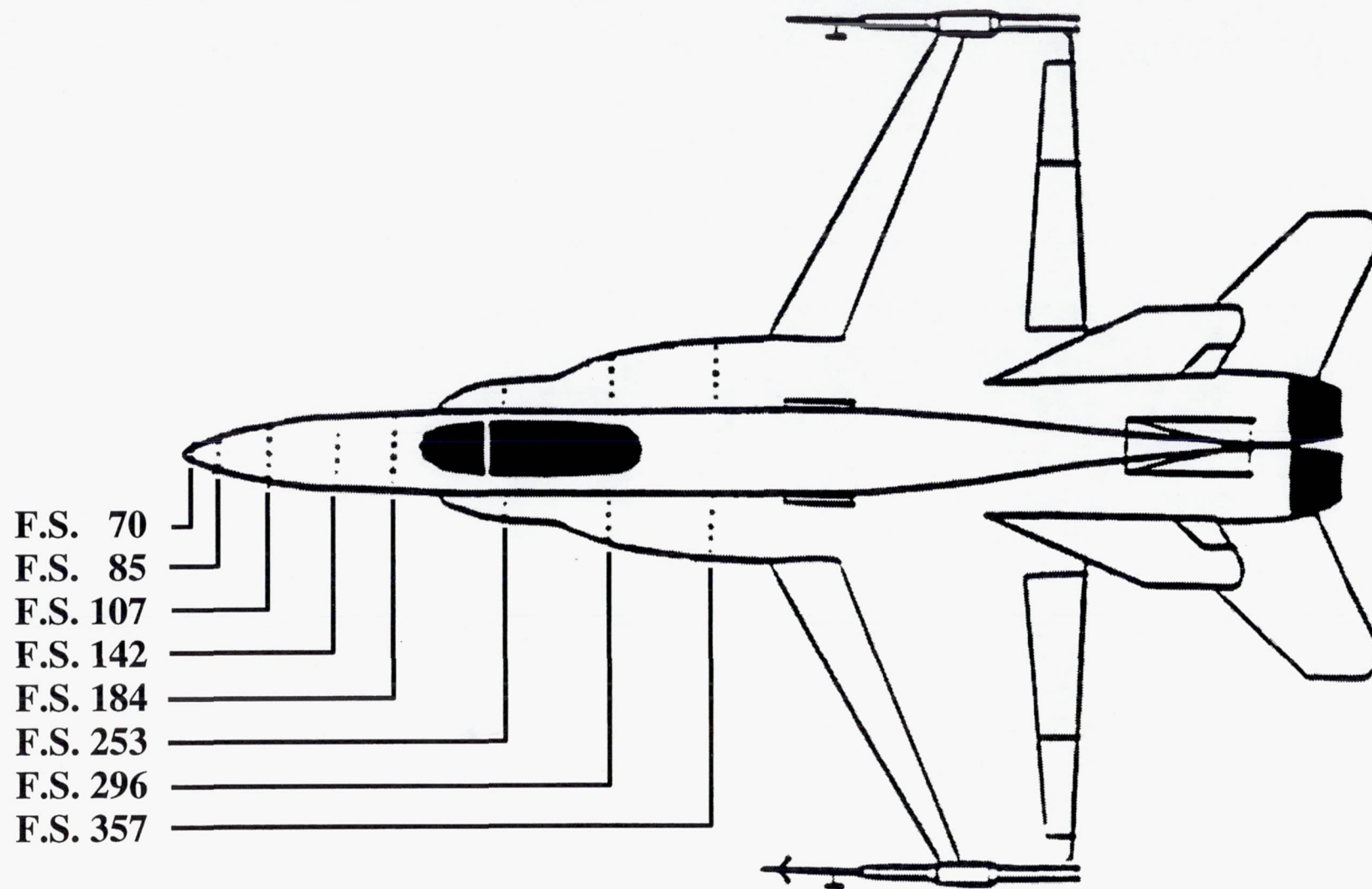


**Fig. 16 – Forebody/LEX Surface Pressure Measurement Stations**



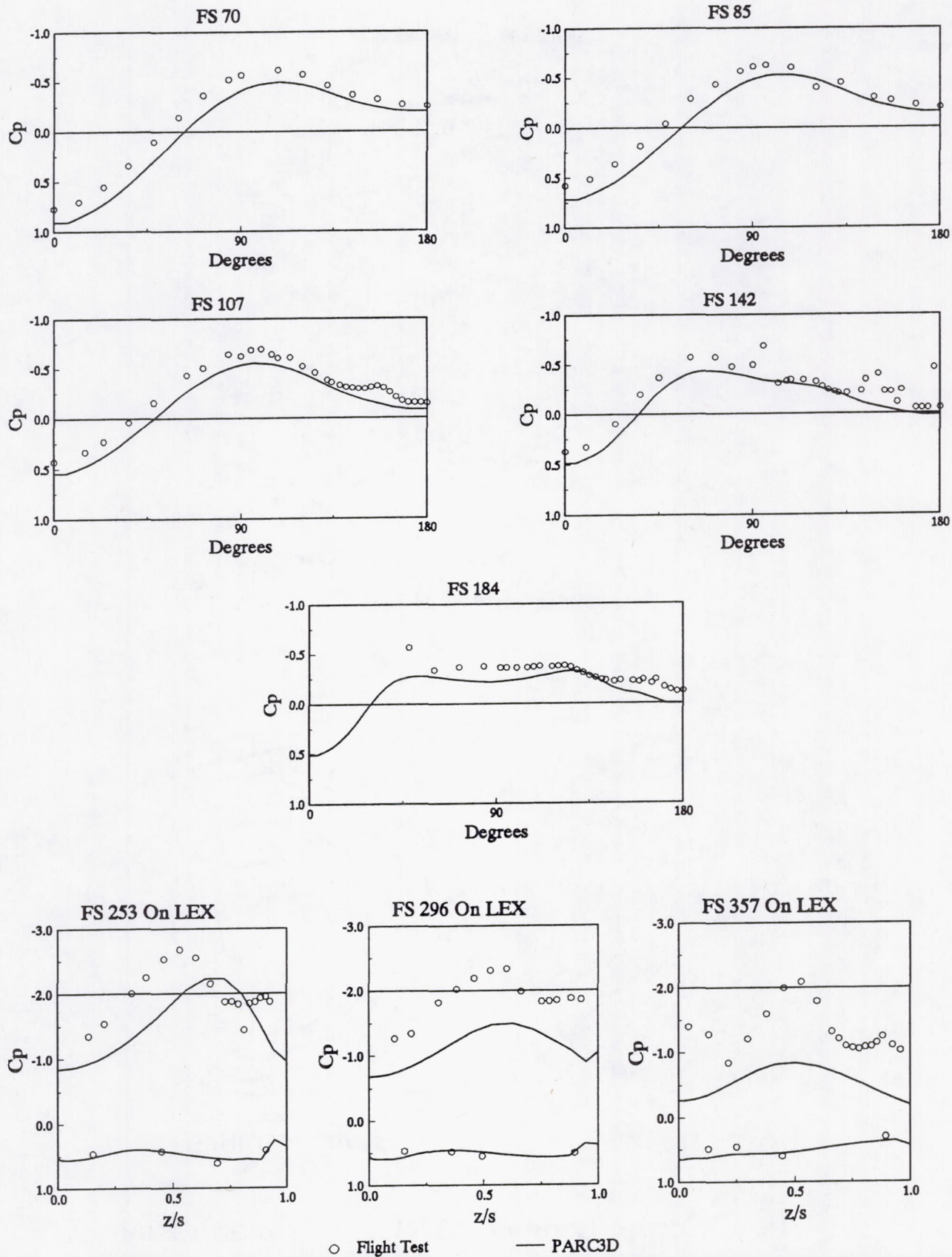
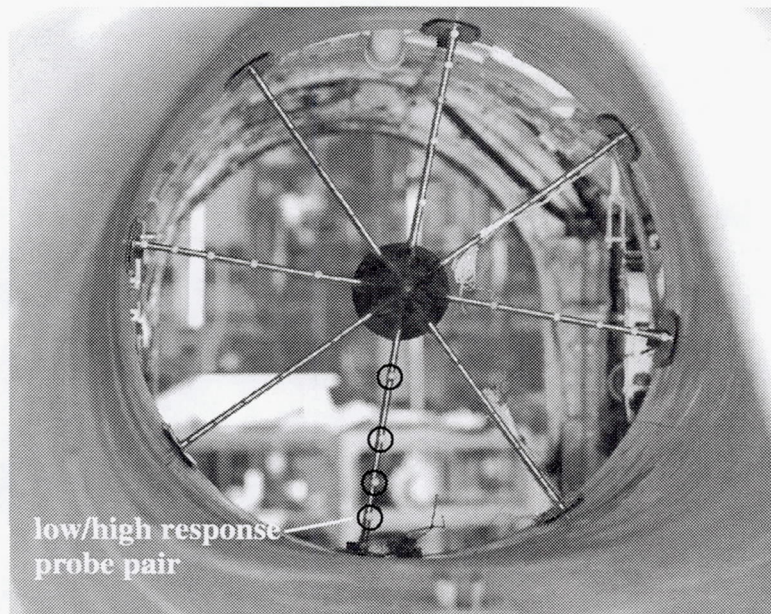
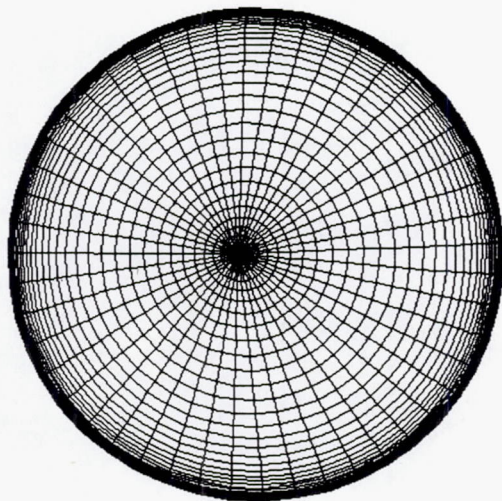


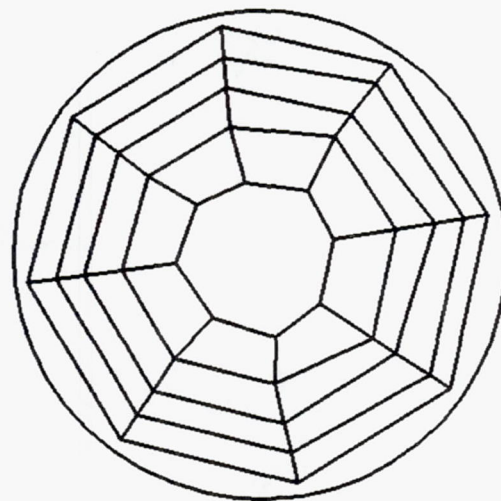
Fig. 17 - Surface Pressure Comparison ( $\alpha = 30^\circ$ , and  $M_\infty = 0.42$ )



**Fig. 18 – F/A-18A HARV Engine Face Pressure Measurement Rake**



**PARC3D Grid**

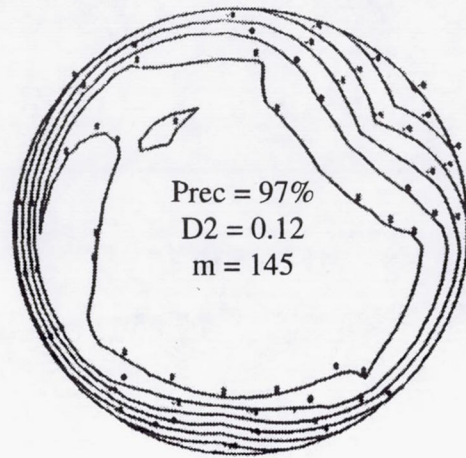


**Rake Simulation**

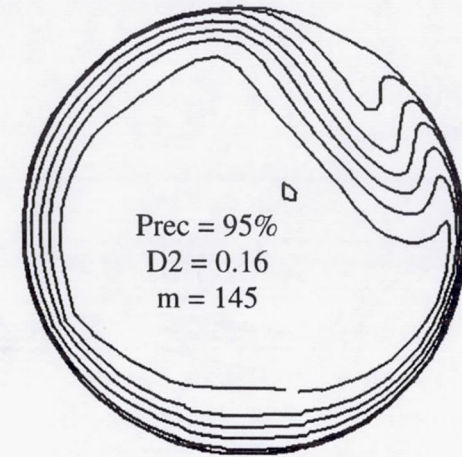
**Fig. 19 – Comparison of PARC3D Grid and Rake**



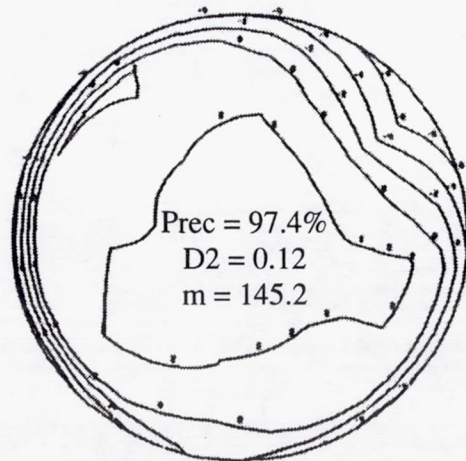
VG out



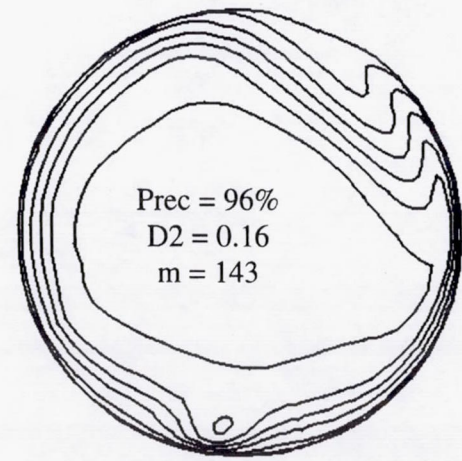
$M/\alpha/\beta = 0.8/3.8/0.0$



VG in



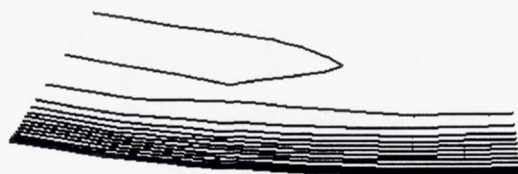
$M/\alpha/\beta = 0.798/3.8/0.0$



FLIGHT TEST  
(dynamic distortion at peak  
fan sensitivity)

PARC3D  
(asymptotic solution)

**Fig. 20 – Effect of Vortex Generators on Total Pressure Contours**



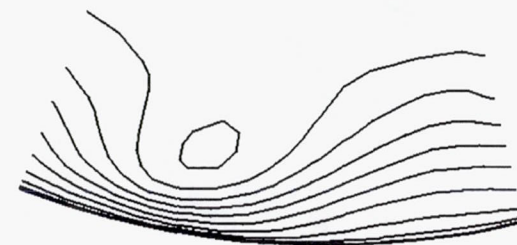
(a)  $x/c = -2.6$



(d)  $x/c = 17.0$



(b)  $x/c = 2.2$



(e)  $x/c = 32.0$



(c)  $x/c = 5.0$



(f)  $x/c = 38.0$

**Fig. 21 – Evolution of Vortex Generators Total Pressure Contours**





(a)  $x/c = -2.6$



(d)  $x/c = 17.0$



(b)  $x/c = 2.2$



(e)  $x/c = 32.0$



(c)  $x/c = 5.0$



(f)  $x/c = 38.0$

**Fig. 22 – Evolution of Total Pressure Contours without VGs**

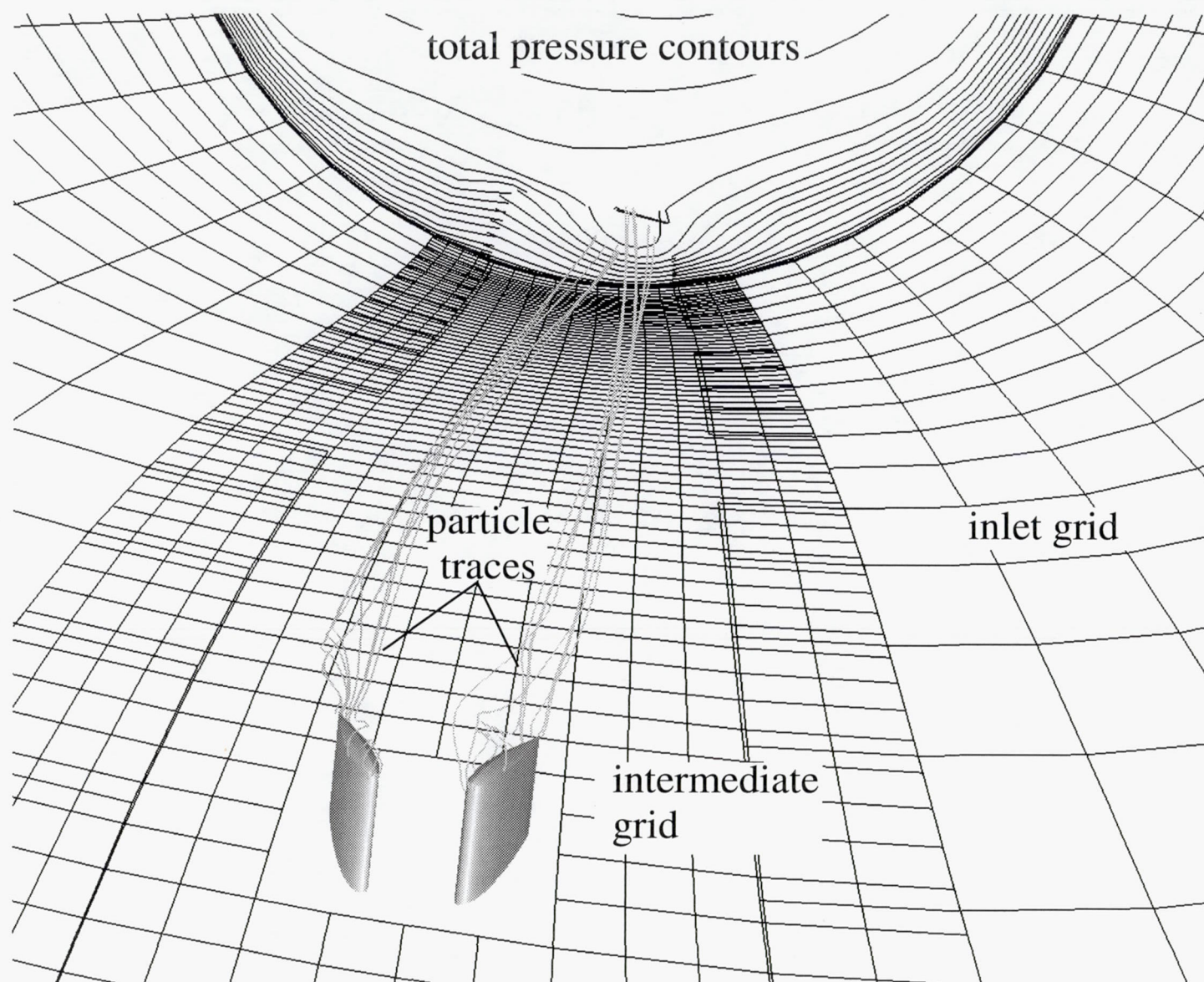


**Fig. 23 – Particle Traces Off Vortex Generators**



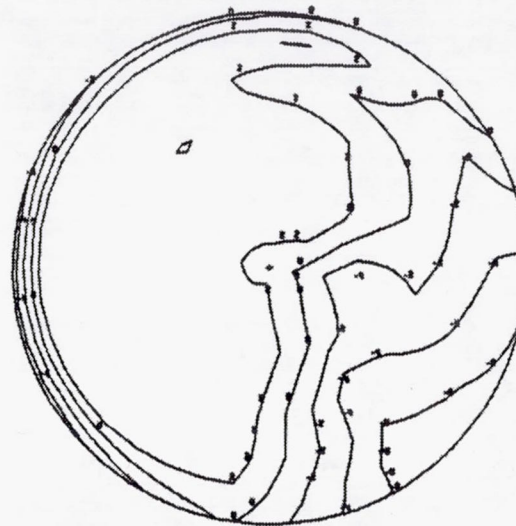
$$M_{\infty} = 0.432$$

$$\alpha = 32.2^{\circ}$$



Prec = 94%  
D2 = 0.17  
m = 144

PARC3D  
(vg)



Prec = 96.5%  
D2 = 0.144  
m = 144.5

Northrup Flight Test  
(at peak distortion)



Prec = 94%  
D2 = 0.16  
m = 143

PARC3D  
(novg)

**Fig. 24 – Effect of Vortex Generators at High Angle of Attack**



(a)  $x/c = -2.6$



(d)  $x/c = 17.0$



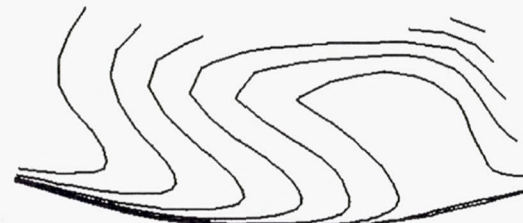
(b)  $x/c = 2.2$



(e)  $x/c = 32.0$



(c)  $x/c = 5.0$



(f)  $x/c = 38.0$

**Fig. 25 – Evolution of Total Pressure Contours with VGs**



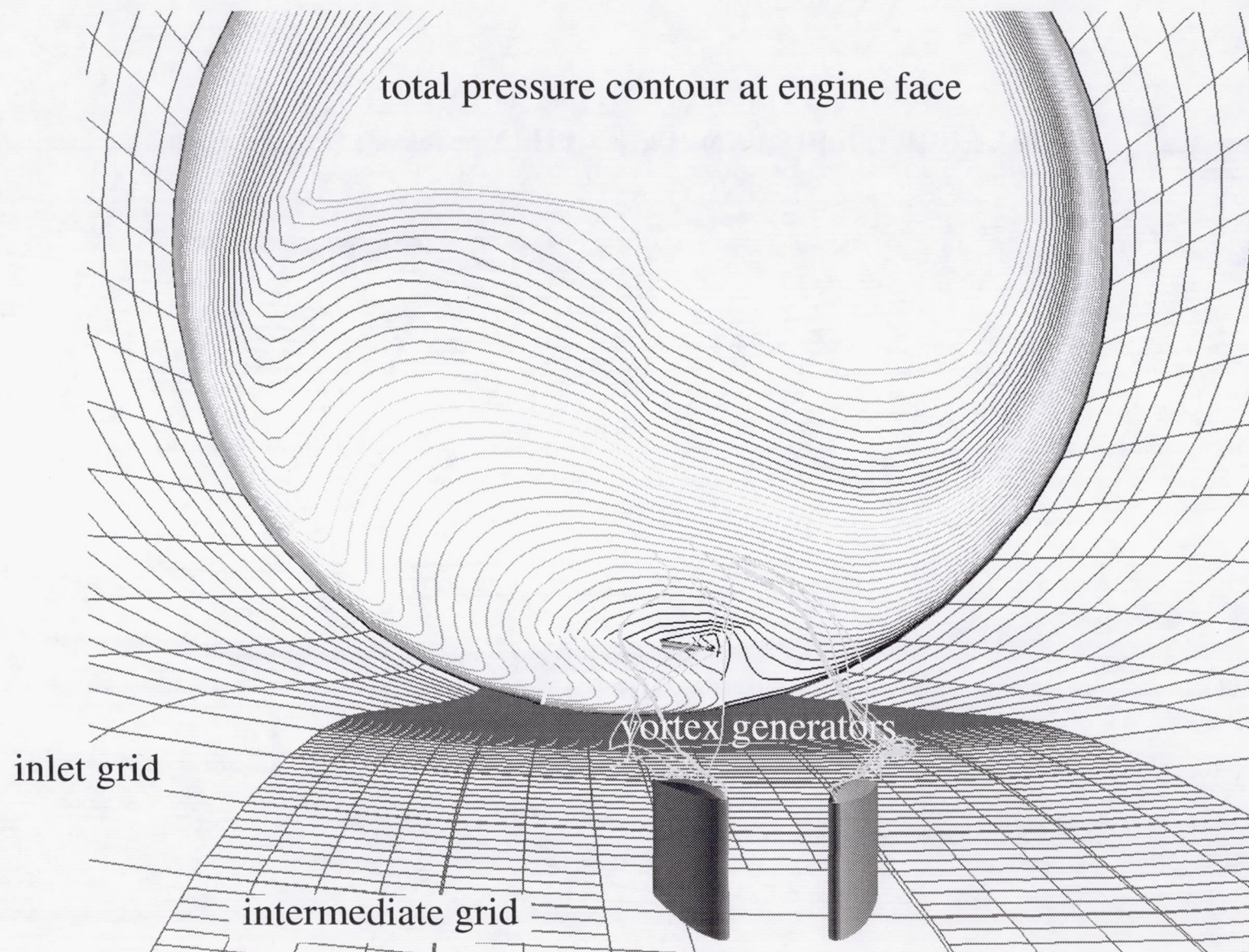


**Fig. 26 – Particle Traces Off Vortex Generators at High Angle of Attack**



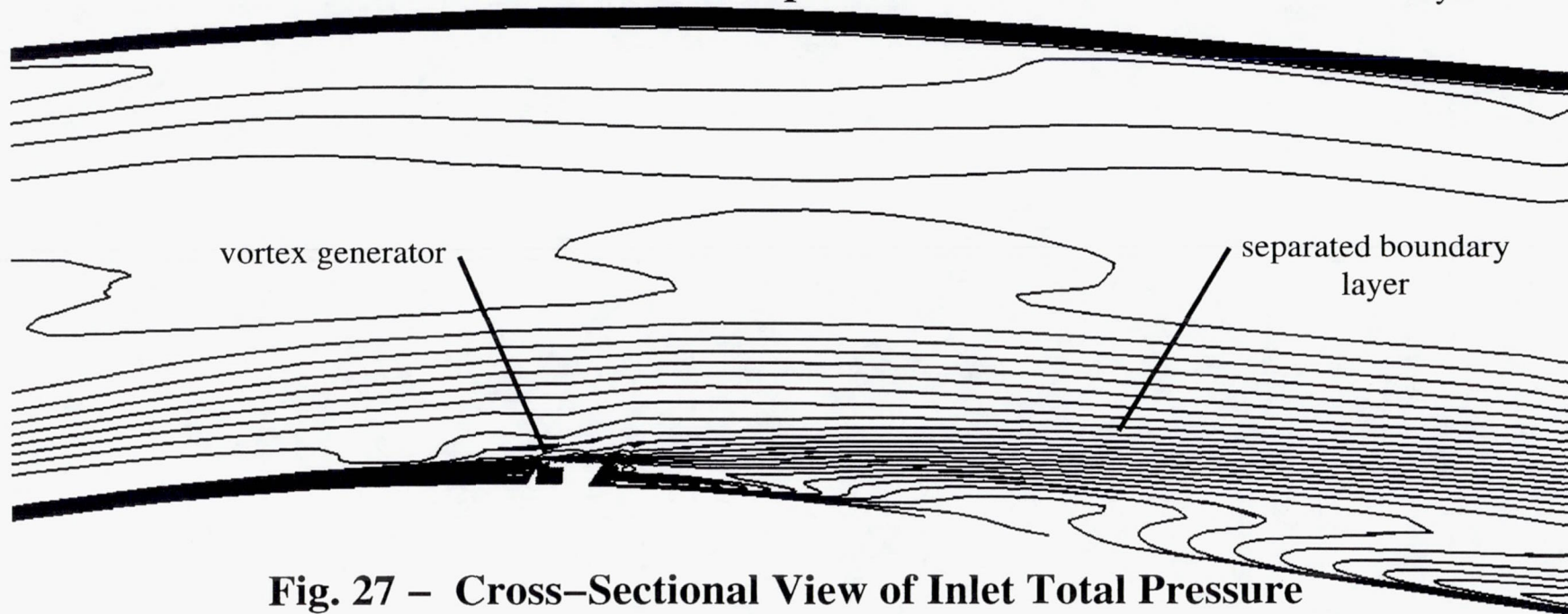
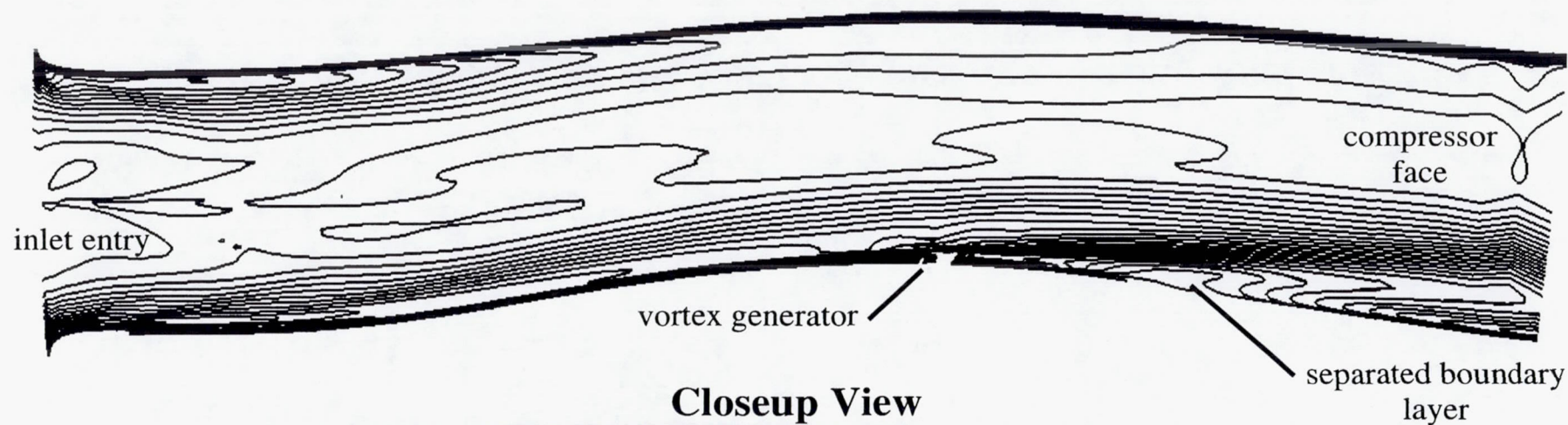


**Fig. 27 – Cross-Sectional View of Inlet Total Pressure Contours at High Angle of Attack**



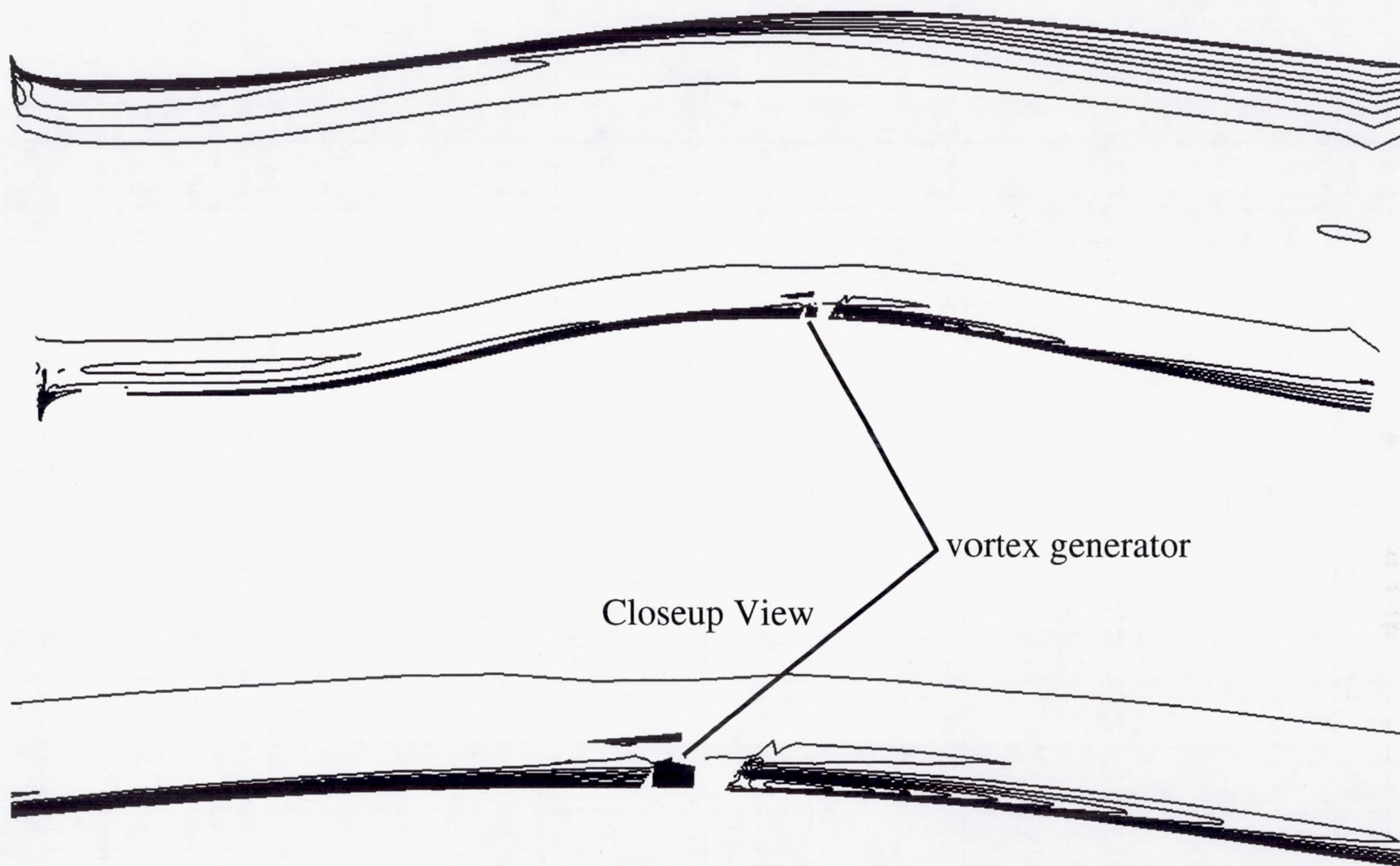


**Fig. 28 – Cross Sectional View of Inlet Total Pressure Contours at High Speed**

REPORT DOCUMENTATION PAGE			Form Approved OMB No. 0704-0188	
Public reporting burden for this collection of information is estimated to average 1 hour per response, including the time for reviewing instructions, searching existing data sources, gathering and maintaining the data needed, and completing and reviewing the collection of information. Send comments regarding this burden estimate or any other aspect of this collection of information, including suggestions for reducing this burden, to Washington Headquarters Services, Directorate for Information Operations and Reports, 1215 Jefferson Davis Highway, Suite 1204, Arlington, VA 22202-4302, and to the Office of Management and Budget, Paperwork Reduction Project (0704-0188), Washington, DC 20503.				
1. AGENCY USE ONLY (Leave blank)	2. REPORT DATE November 1995	3. REPORT TYPE AND DATES COVERED Final Contractor Report		
4. TITLE AND SUBTITLE  PARC3D Calculations of the F/A-18A HARV Inlet Vortex Generators		5. FUNDING NUMBERS  WU-505-68-30 C-NAS3-27186		
6. AUTHOR(S)  Steve D. Podleski				
7. PERFORMING ORGANIZATION NAME(S) AND ADDRESS(ES)  NYMA, Inc. 2001 Aerospace Parkway Brook Park, Ohio 44142		8. PERFORMING ORGANIZATION REPORT NUMBER  E-9744		
9. SPONSORING/MONITORING AGENCY NAME(S) AND ADDRESS(ES)  National Aeronautics and Space Administration Lewis Research Center Cleveland, Ohio 44135-3191		10. SPONSORING/MONITORING AGENCY REPORT NUMBER  NASA CR-195456		
11. SUPPLEMENTARY NOTES  Project Manager, Thomas J. Biesiadny, Propulsion Systems Division, NASA Lewis Research Center, organization code 2780, (216) 433-3967.				
12a. DISTRIBUTION/AVAILABILITY STATEMENT  Unclassified - Unlimited Subject Category 07  This publication is available from the NASA Center for Aerospace Information, (301) 621-0390.			12b. DISTRIBUTION CODE	
13. ABSTRACT (Maximum 200 words)  NASA Lewis Research Center is currently engaged in a research effort as a team member of the High Alpha Technology Program within the NASA agency. This program uses a specially-equipped F/A-18A aircraft called the High Alpha Research Vehicle (HARV), in an effort to improve the maneuverability of high-performance military aircraft at low-subsonic-speed, high-angle-of-attack conditions. The overall objective of the NASA Lewis effort is to develop inlet analysis technology towards efficient airflow delivery to the engine during these maneuvers. One portion of this inlet analysis technology uses computational fluid dynamics to predict installed inlet performance. Most of the F/A-18A HARV geometry, which includes the ramp/splitter plate, side diverter and slot, inlet lip and upper diverter, and deflected leading-edge flap has been modeled. The empennage and rear fuselage has not. A pair of vortex generators located on the bottom wall of the inlet were not modeled initially. These vortex generators were installed to alleviate any flow separation that may be induced by the wheel well protrusion into the inlet wall. Calculations completed with the PARC3D code showed that the pressure recovery has been underpredicted and the flow distortion overpredicted. To improve the correlation of PARC3D predictions with flight and wind tunnel tests, the vortex generators were included in the grid geometry and their results are presented in this report. The grid totals 27 blocks or 1.3 million grid points for the half model, which includes the vortex generator grid blocks. Two flight cases were calculated, a high speed case with a Mach number of 0.8 and angle of attack of 3.4°; and a low speed case with a Mach number of 0.43 and angle of attack of 32.3°. The vortex generators have a significant effect on the inlet boundary layers at high speed, low angle of attack; and have no effect at low speed, high angle of attack.				
14. SUBJECT TERMS  Vortex generators; F/A-18; Inlet; High angle of attack; Separated flow			15. NUMBER OF PAGES 56	
			16. PRICE CODE A04	
17. SECURITY CLASSIFICATION OF REPORT Unclassified	18. SECURITY CLASSIFICATION OF THIS PAGE Unclassified	19. SECURITY CLASSIFICATION OF ABSTRACT Unclassified	20. LIMITATION OF ABSTRACT	